Interactive comment on “The optical, physical properties and direct radiative forcing of urban columnar aerosols in Yangtze River Delta, China”

by Bingliang Zhuang et al.

Anonymous Referee #2

Received and published: 19 July 2017

To anonymous Referee #2:

Dear reviewer, thank you very much for dedicating time to review the manuscript and provide us the important comments and suggestions on our study. We have learned a lot from your advices and made great efforts to improve the manuscript accordingly. A carefully point by point response to your comments has been listed below. The revised details can be referred to the new version of the manuscript.

Relevant changes of the revised manuscript (marked with traces) are also enclosed in the last part of this document.

General comments

This measurement-based study analyzes the column-integrated optical and physical properties and direct radiative effects (DRE) of aerosols in Nanjing. The authors present the mode (coarse and fine) and composition (scattering and absorbing)-dependent aerosol optical properties, with some properties directly measured and some inversely derived. They also present and discuss the seasonal variation of the aerosol optical and physical properties and direct radiative effects.

The major concern is the novelty of the study. It appears that considerable studies have been conducted on the column-integrated aerosol properties and DRE in this region, especially the authors have published several papers in this topic and in this region. What presents in the manuscript is more like a synthesis of what the authors and others have done with an extension of the time coverage, and it is hard to find anything new.

R: We sincerely thanks for your comments. For this one, I'm afraid the authors can't agree with you that the manuscript is just a synthesis of previous publications with an extension of the time coverage.

1. Indeed, some researches on the column-integrated aerosol optical properties have been carried out in most sites of YRD recently. However, almost all of them focus on the aerosol optical properties in the **coast, lake and rural** regions (*Pan et al.*, 2010; *Yu et al.*, 2011; *Che et al.*, 2015a; *Qi et al.*, 2016) in central to east YRD. And most of them only address the total aerosol optical properties (independent of modes and compositions) except *Qi et al.*, (2016), who also made an introduction on the aerosol physical parameters and size fractional SSA in **eastern coast** city (Hangzhou) of YRD. Hangzhou is about 300 km far away from Nanjing. As implied in *Zhang et al.* (2012), aerosols are complicated in compositions and spatial distributions especially in fast developing regions with intense human activities (such as YRD). Thus, large differences of the aerosol optical and physical properties might exist to degrees among the sites within YRD. Additionally, none of researches mentioned above have

studied the aerosol radiative forcing (DRF), which is the basic premise of understanding the aerosol climate effects. Therefore, it's still necessary to investigate the column-integrated aerosol optical and physical properties, as well as their radiative effects in urban area of **west YRD**.

2. Indeed, the authors have carried out a series of studies on the aerosols in Nanjing (such as Zhuang et al., 2014; 2015 and 2017). However, most of them (Zhuang et al., 2015; 2017) only address the surface aerosol optical properties which are very different from the column-integrated aerosols. Surface data could not completely represent the whole aerosol properties in atmosphere and they are highly affected by the variations of boundary layers. While in Zhuang et al. (2014), the column-integrated scattering and absorbing aerosol optical properties with split modes, the size fractional aerosol physical properties and the fractionated aerosol DRFs of different aerosol (scattering, absorbing and the total) components in west YRD have not been investigated or estimated (undressed issues). By comparisons: **I).** this study considers all the undressed issues in Zhuang et al. (2014) (and in other studies) mentioned above to make us better understand the aerosol properties and DRFs in west YRD. **II).** It further quantifies the aerosol classifications or mixings (dust and black carbon aerosol affections) in urban area of west YRD by analyzing the relationships among the aerosol optical properties. **III).** And it also quantifies the influence or importance of the aerosol profile on the assessment of the aerosol DRFs in clear sky condition, which could be as a reference for the study of the aerosol DRF uncertainty. **IV).** The DRFs in this study might be more precise because, in previous research (Zhuang et al., 2014), they (the whole mode DRFs) were calculated using the default aerosol profile of the model instead of the observed ones. And the absorb DRF, which might be underestimated, were estimated based on fresh BC SSAs in theirs. In brief, all these items have not been addressed in authors' previous researches; neither did in other studies in YRD or east China.

3. Back to the time coverage, the authors believe that a larger data set or longer sampling period, not the novelty of the study, but would make the results more representativeness especially for the climate researches.

Overall, this manuscript presents more comprehensive, systematic and deeper analysis on the aerosol optical, physical and radiative properties in urban area of west YRD. Results further indicate the characteristics of the aerosol properties and reveal the contributions of each component in different size segments to the total aerosol AODs and DRFs in west YRD. And they are also advantageous to improve the model performances on the aerosol and its effects in east regions of China.

According to your comments, doubts and suggestions, the manuscript has been rephrased throughout the whole text. The novelty (listed above) and finding(s) of this study have been refined in better ways of expression, which could be shown in most parts of the revised manuscript, including in the sections of Abstract, Introduction, Discussions, as well as Conclusion. Details can be found in the revised manuscript.

Reference:

Che, H. Z., Zhang, X. Y., Xia, X., Goloub, P., Holben, B., Zhao, H., Wang, Y., Zhang, X. C., Wang, H., Blarel, L., Damiri, B., Zhang, R., Deng, X., Ma, Y., Wang, T., Geng, F., Qi, B., Zhu, J., Yu, J., Chen, Q., and Shi, G..: Ground-based aerosol climatology of China: aerosol optical depths from the China Aerosol Remote Sensing Network (CARSNET) 2002–2013, Atmos. Chem. Phys., 15, 7619–7652, 2015a.

Pan, L, Che, H. Z., Geng, F. H., Xia, X. A., Wang, Y. Q., Zhu, C. Z., Chen, M., Gao, W., and Guo, J.

P.: Aerosol optical properties based on ground measurements over the Chinese Yangtze Delta Region, Atmos. Environ., 44, 2587-2596, doi:10.1016/j.atmosenv.2010.04.013, 2010.

Qi, B., Hu, D. Y., Che, H. Z., Du, R. G., Wu, Y. F., Xia, X. A., Zha, B., Liu, J., Niu, Y. W., Wang, H., Zhang, X. Y., and Shi, G. Y.: Seasonal variation of aerosol optical properties in an urban site of the Yangtze Delta Region of China. Aerosol Air Qual. Res., 16, 2884-2896, 2016.

Yu, X. N., Zhu, B., Yin, Y., Fan, S. X., and Chen, A. J.: Seasonal variation of columnar aerosol optical properties in Yangtze River Delta in China, Adv. Atmos. Sci., 28(6), 1326-1335, doi:10.1007/s00376-011-0158-9, 2011.

Zhang, X. Y., Wang, Y. Q., Niu, T., Zhang, X. C., Gong, S. L., Zhang, Y. M., and Sun, J. Y.: Atmospheric aerosol compositions in China: Spatial/temporal variability, chemical signature, regional haze distribution and comparisons with global aerosols, Atmos. Chem. Phys., 12, 779–799, doi:10.5194/acp-12-779-2012, 2012.

Zhuang, B. L., Wang, T. J., Li, S., Liu, J., Talbot, R., Mao, H. T., Yang, X. Q., Fu, C. B., Yin, C. Q., Zhu, J. L., Che, H. Z., and Zhang, X. Y.: Optical properties and radiative forcing of urban aerosols in Nanjing, China, Atmos. Environ., 83, 43–52, 2014.

Zhuang, B. L., Wang, T. J., Liu, J., Ma, Y., Yin, C. Q., Li, S., Xie, M., Han, Y., Zhu, J. L., Yang, X. Q., and Fu, C. B.: Absorption coefficient of urban aerosol in Nanjing, west Yangtze River Delta, China, Atmos. Chem. Phys., 15, 13633–13646, 2015.

Zhuang, B. L., Wang, T. J., Liu, J., Li, S., Xie, M., Han, Y., Chen, P. L., Hu, Q. D., Yang, X. Q., Fu, C. B., Zhu, J. L.: The surface aerosol optical properties in urban area of Nanjing, west Yangtze River Delta, China, Atmos. Chem. Phys., 17, 1143–1160, 2017.

In addition, the manuscript is quite dully lengthy, and for the way it is presented, I feels that the results/findings are somewhat isolated and trivial, and I find it difficult to grasp useful information in the context of its contribution to the current understanding of the aerosol radiative effects and model applications to reduce the uncertainty in estimating the aerosol DRE.

R: Thanks a lot for figuring out the problems of the manuscript's writings. With respect to your comments, the manuscript has been rephrased significantly and shortened in necessarily throughout the whole text. And it's believed that the revised version of the manuscript is much more clearly and readable. The readers would more easily grasp the useful information of the results. For example, this study quantifies the DRFs of different aerosol components in different size segments and further reveals their contributions to the totals. And the results are also much more echoed from each other than those in original version of manuscript.

In revised manuscript, the authors also highlight the importance of the aerosol properties to improve the model performance. **1.** The most directly use of the data, including the estimated DRF, is available to validate the numerical simulations. **2.** The observed aerosol optical and physical properties could be used for data assimilation to grasp better inputs (initial conditions and variations of emissions) of the models. This is advantageous to obtain more precise aerosol loadings and subsequently its radiative forcing in corresponding regions. **3.** The data set of the optical properties in most of the climate or air quality models are frequently from a given refractive index which is homogeneous in time and space. Therefore, a more precise aerosol refractive index used in numerical models would yield a more reasonable aerosol optical properties and radiative forcing in observed regions and around. **4.** A more precise aerosol size distribution would also make the models more accurate in describing the aerosol physical processes (transportation, deposition) and radiative effects. All these statements (including

corresponding references) have been included in the revised manuscript.

Finally, many aerosol properties are retrieved through an inverse algorithm in which measurement errors and assumptions are critical. The authors do not specify what are the errors and assumptions, and fail to discuss how they would affect the uncertainties in the derived variables.

R: Thanks for your comments and suggestions. As indicated in Introduction section, the column-integrated aerosol optical and physical properties from CE-318 have been widely used and investigated globally; implying that the retrieval algorithm is mature and relevant products could meet the precision requirements to degrees. Many studies have presented the detailed introduction on the inverse algorithm (such as in *Dubovik et al.*, 2000; 2006*; Yu et al.*, 2010; etc.) and reported relevant errors or uncertainties of the products. Therefore, the subsequent studies (such as in *Eck et al.*, 2010; *Li et al.*, 2015) directly cited the existing references when introducing the observed errors of the aerosol properties from CE-318, instead of detailed repeating the progresses to avoid duplication. Similarly, the revised manuscript supplements the uncertainties of the inversed aerosol variables in Section 2.1 and the influence ways could not be repeated, but directly cite the corresponding references mentioned above.

Additionally, effects of the uncertainties from measurements on the aerosol DRFs are further discussed in Section 3.4.3 of the revised manuscript.

Reference:

Dubovik, O. and King, M. D.: A flexible inversion algorithm for the retrieval of aerosol optical properties from Sun and sky radiance measurements, J. Geophys. Res., 105, 20673–20696, doi:10.1029/2000JD900282, 2000.

Dubovik, O., Sinyuk, A., Lapyonok, T., Holben, B. N., Mishchenko, M., Yang, P., Eck, T. F., Volten, H., Munoz, O., Veihelmann, B., van der Zande, W. J., Leon, J. F., Sorokin, M., and Slutsker, I.: Application of spheroid models to account for aerosol particle nonsphericity in remote sensing of desert dust, J. Geophys. Res.-Atmos., 111, D11208, doi:10.1029/2005jd006619, 2006.

Eck, T. F., et al. (2010), Climatological aspects of the optical properties of fine/coarse mode aerosol mixtures, J. Geophys. Res., 115, D19205, doi:10.1029/2010JD014002.

Li, J., B. E. Carlson, and A. A. Lacis (2015), Using single-scattering albedo spectral curvature to characterize East Asian aerosol mixtures, J. Geophys. Res. Atmos., 120, 2037–2052, doi:10.1002/2014JD022433.

Yu, X. N., Zhu, B., Yin, Y., Fan, S. X., and Chen, A. J.: Seasonal variation of columnar aerosol optical properties in Yangtze River Delta in China, Adv. Atmos. Sci., 28(6), 1326-1335, doi:10.1007/s00376-011-0158-9, 2011.

Due to these issues, the current form of the manuscript is not suitable for publication.

R: With respect to your comments and suggestions, significant revisions and improvements of the manuscript have been made. And it is believed that the revised manuscript may have potential for publication.

The optical, physical properties and direct radiative forcing of urban columnar aerosols in Yangtze River Delta, China

Bingliang Zhuang[1, *], Tijian Wang[1, **], Jane. Liu[1,2], Huizheng Che[3], Yong Han[1], Yu Fu[4], Shu Li[1], Min Xie[1], Mengmeng Li[1], Pulong Chen[1], Huimin Chen[1], Xiu-qun Yang[1], Jianning Sun[1]

[1] School of Atmospheric Sciences, CMA-NJU Joint Laboratory for Climate Prediction Studies, Jiangsu Collaborative Innovation Center for Climate Change, Nanjing University, Nanjing 210023, China

[2] Department of Geography and Planning, University of Toronto, Toronto, M5S 3G3, Canada

[3] Key Laboratory of Atmospheric Chemistry (LAC), Chinese Academy of Meteorological Sciences (CAMS), CMA, Beijing, 100081, China

[4] Dalian Weather Modification Office, Dalian, 116001, China

[*] Corresponding author, E-mail: blzhuang@nju.edu.cn; Tel.: +862589681156; fax: +862589683797

[* *]Corresponding author, E-mail: tjwang@nju.edu.cn; Tel.: +862589683797; fax: +862589683797

Abstract: The fractionated aerosol optical and physical properties as well as its direct radiative forcing (DRF) in urban area of west Yangtze River Delta (YRD)~~Nanjing (urNJ)~~ are investigated, based on the measurements of Cimel sun-photometer combined with a radiation transfer model. Ground based observed aerosols have much higher temporal resolutions compared with satellite retrievals. Analysis firstly reveals the characteristics of fractionated aerosol optical properties of different aerosol types in west YRD. ~~We find that t~~The annual mean ~~550 nm aerosol~~ optical depth ~~(AOD)~~ of the total aerosols is ~~about~~ 0.65±0.28, dominated by the scattering aerosols (~~about 94%~~93.8%), with a mean refractive index of 1.44+0.0084i at 440 nm. ~~resulting in a mean single scattering albedo (SSA) of 0.93 at 550 nm and refractive index of 1.44+0.0084i at 440 nm during the sampling period.~~ The fine aerosols are about 4 times to, and also have very different compositions from the coarse ones. The absorbing components

only account for ~4.6% in fine aerosols while 15.5% in coarse aerosols, but within the same mode, they have smaller sizes than scattering aerosols. ~~The scattering aerosol has larger size than the absorbing aerosol, with Ångström exponents (AE) of 1.19 at 440/870 nm, 0.13 smaller than the latter one. The coarse mode fraction for the scattering aerosol (18.03%) is much smaller than the absorbing aerosol's (43.91%).~~ Therefore~~us~~, the fine ~~mode aerosols~~particles are much ~~presents more~~ scattering ~~(SSA=0.95) while~~than the coarse ones~~aerosol is more absorption (SSA=0.82)~~, simultaneously reflecting that each component has different size distributions. Relationships among the optical properties quantify the aerosol mixings and they imply ~~Analysis implies that there are~~ about 15% and 27.5% occurrences of dust and black carbon dominated mixing aerosols, respectively, ~~during the sampling period~~in west YRD. Different from optical properties, aerosols in west YRD have the similar volume size distributions to the ones in other sites over east China climatologically. ~~All the optical properties follow a simple unimodal pattern. Aerosols in urNJ have a two-mode lognormal pattern in volume size distribution,~~ peaking at the radius of 0.148 and 2.94 μm~~, and the AOD positively depends on them~~. But analysis further reveals that the fine or coarse dominated particles could individually lead to severe haze pollutions in YRD.~~Although the fine mode aerosol has a much smaller sizes than the coarse one, they have the same level of the volume concentrations (about 0.12 $\mu m^3/cm^3$) due to much higher fraction of the fine aerosol.~~ Observed based estimations indicate that both the fine and coarse aerosols in west YRD exert a negative DRF, especially for the former one (-11.17 W/m^2 at the top of atmosphere, TOA). A higher absorption fraction directly leads to the negative DRF being offset more substantially for coarse aerosols (-0.33 W/m^2) at the TOA. Similarly, the coarse mode DRF only contributes to ~14% within scattering aerosols while >34% witnin absorbing aerosols. ~~Estimations present that the mean aerosol DRFs at the top of atmosphere (TOA) are -10.69, -16.45, +5.76 W/m^2, respectively, for the total,~~

~~scattering and absorbing aerosols in clear sky. At the surface, the DRFs are 1.1-2.5 times stronger than those at TOA, and the fine aerosol DRFs in these three type of aerosols account for 83.7%, 91.7% and 67.2%, respectively, to their totals.~~ Sensitive analysis states that~~Normally,~~ aerosol DRFs is not very sensitive ~~(no more than 5%)~~ to its profiles in clear sky condition ~~(extreme cases excepted), although both aerosol scattering and absorption could become weaker to some extent if more aerosols were in lower layers~~. Both the aerosol properties and DRFs have substantial seasonality in west YRD. Results further reveal the contributions of each component in different size segments to the total AODs and DRFs. Also they are advantageous to improve the model performances on the aerosol and its effects in east regions of China.

1 Introduction

Atmospheric aerosols have significant influences on air quality, human health, and regional/global climate changes. Their loadings in the global atmosphere have increased substantially ~~in recent years~~. Scientists suggested that the scattering aerosols~~, such as sulfate and nitrate,~~ could greatly offset the warming effects of greenhouse gases (Kiehl and Briegleb, 1993) while the absorbing ~~aerosols~~components~~, such as black carbon (BC),~~ might further exacerbate the global warming (Jacobson 2002). The global mean direct radiative forcing~~s~~ (DRF) of scattering aerosols, fossil fuel BC and the total aerosols ~~were~~ was estimated to be about -0.55, +0.2, -1.04 W/m^2, respectively (Forster et al., 2007; Reddy et al., 2005~~).~~) at the top of atmosphere (TOA), thus changing t~~T~~he atmospheric circulations and hydrological cycle ~~would be further affected when the radiation balance is changed by the aerosols~~. Menon et al. (2002) suggested that changes in the trend of rainfall in China over the past 5 decades might be related to the variation of BC in ~~southern and eastern~~ Asia regions. Wang et al. (2015)

indicates that the East Asia summer monsoon circulation could become weaker due to the cooling effects of the aerosols but stronger due to the warming effects of BC.

Although many studies on the aerosol radiative forcing and climate effects have been carried out in both global and regional scales based on model simulations and observations in the past two decades (e.g., Penner et al., 2001; Bellouin et al., 2003; Liao and Seinfeld, 2005; Wu et al., 2012; Wang et al., 2015; etc.), large uncertainties still exist. Forster et al. (2007) pointed out that the global mean ~~direct radiative forcing~~DRF varied from +0.04 to -0.63 W/m^2 for the total aerosols and from +0.1 to +0.3 W/m^2 for BC. The ranges were larger in regional scales, especially in high aerosol emitted regions (Zhuang et al., 2013a). ~~Zhuang et al. (2013a) indicated that the simulated BC direct raidative forcing varied from +0.32 to +0.81 W/m^2 over East Asia.~~ The DRF uncertainties would subsequently result in large bias ~~when assessing~~of the aerosol climate effects. There are many ~~key~~ factors affecting the simulated radiative forcing, including ~~are~~ the aerosol optical properties, which are related to the aerosol emissions, size distributions, profiles, compositions, and mixing states (Holler et al., 2003; Ma et al., 2017), surface albedo and clouds (Ma and Yu, 2012; Forster et al., 2007). The uncertainties could be reduced substantially if the observed aerosol optical properties were figured out and ~~were~~ used ~~when calculating the forcing~~ (Forster et al., 2007).

With the rapid increase in population and growth in economics, the air pollutant~~trace gases and particulate matter~~ emissions are much higher in East Asia than in the other regions (Zhang et al., 2009). Additionally, dust aerosols from desert regions~~northwest China and Mongolia~~ are always transported to north and east China or even further afield (Wang et al., 2009; Sun et al., 2012; Li et al., 2015a). Consequently, aerosols in China become frequently large in loadings and complicated in compositions and spatial distributions (Zhang et al., 2012), especially in urban agglomerations or megacities (e.g.:

Yangtze River Delta: YRD). Therefore, it is necessary to clarify ~~study~~ the aerosol optical properties ~~and radiative forcing~~ in YRD through observations, which is a premise for accurately estimating the aerosol radiative ~~climate~~ effects and also in favor of improving the model performance on aerosols ~~–~~in ~~East~~ east region of China~~Asia~~. Recently, substantial observation-based studies have conducted on both the surface (e.g., Bergin et al., 2001; Xu et al., 2002; Zhang et al., 2004; Xia et al., 2007; Yan et al., 2008; He et al., 2009; Fan et al., 2010; Cai et al., 2011; Xu et al., 2012; Wu et al., 2012; Zhang et al., 2015; Yu et al., 2016; Deng et al., 2016; etc.) and columnar (e.g., Chiang et al., 2007; Pan et al., 2010; Yu et al., 2011; Zhao et al., 2013; Tao et al., 2014; Zhu et al., 2014; Che et al., 2011; 2013; 2014; 2015a, b, c; Xia et al., 2016; Zheng et al., 2016; Qi et al., 2016, etc.) aerosol optical properties (and ~~direct radiative forcing~~DRFs), especially ~~on aerosols~~ in China. However, surface data could not completely represent the whole conditions of the aerosols in atmosphere and they are highly affected by the variations of boundary layers. Its deficiency could be made up by the measurements of the columnar aerosols. For the studies of surface aerosols, people mainly focus on their absorption and scattering coefficients (AAC and SC). Investigations state that ~~the annual mean aerosol absorption coefficient (AAC) at 532 nm was about 56 Mm^{-1} in urban area of Beijing from 2005 to 2006 (He et al. 2009) and it was about 41~44 Mm^{-1} at an urban site of YRD from 2012 to 2013 (Zhuang et al., 2015). The annual mean aerosol scattering coefficients (SC) at 520 nm and AAC at 532 nm were 525 and 83 Mm^{-1}, respectively, in Xi'an in 2009 and were 456 and 96 Mm^{-1}, respectively, in Chengdu in 2011. B~~both AACs and SCs in urban areas are frequently stronger than those at other sites. They ~~AAC and SC~~ were ~~17.5~~~30 and ~~174.6~~338 Mm^{-1} in ~~rural area of Beijing~~west YRD (~~Yan et al., 2008~~Zhuang et al., 2017) ~~and they were 6 and 158 Mm^{-1}, respectively in desert region (Xu et al., 2004)~~. For columnar aerosol observations~~s~~, the detailed aerosol optical and physical properties could be obtained, including optical depth (AOD),

refractive index, Ångström exponents (AE), and so on. Che et al. (2015a) introduced a systematic long-term measurement of the countrywide total aerosol AOD and AE in China from 2002 to 2013, and indicated that annual mean AOD were 0.14, 0.74 and 0.54 at the rural sites, urban sites, and in east China, respectively. In YRD, Pan et al. (2010) shows that ~~optical depths (~~AOD~~)~~ at 440 nm and ~~Ångström exponents (~~AE~~)~~ in coastal area (east YRD) ~~of the Yangtze River Delta (YRD)~~ was about 0.74 and 1.27, respectively. Yu et al. (2011) and Qi et al. (2016) indicate~~s~~ that the total aerosol AOD ~~and aerosol scattering albedo (SSA) in the lake areas of the YRD~~ exceeded 0.6 and its single scattering albedo (SSA) was ~~and~~ ~0.88~~, respectively,~~ in lake and urban areas of central to east YRD~~with significant seasonality, while in Hangzhou, they were larger than 0.72 and 0.89, respectively (Qi et al., 2016). In addition to east China, Che et al. (2011, 2013), Zhao et al. (2013), Zhu et al. (2014), Tao et al. (2014) and Yu et al. (2015) investigated the columnar aerosol optical properties in Waliguan Mt. area, Taklimakan Desert, industrial region of northeast China, north China (which can be taken as a region with the background aerosol), the Sichuan Basin in southwest China and desert region of northwest China, respectively. In 2015, Che et al. (2015a) initiated a systematic long-term measurements of the countrywide AOD and AE in China from 2002 to 2013, including 4 remote sites, 25 rural sites, 21 urban sites. Their results showed that annual mean AOD were 0.14, 0.74 and 0.54 at the rural sites, at the urban sites, and in east China, respectively.~~ Zhuang et al. (2014a) indicates that a one-year observed AOD and AE of the total aerosols in urban area of Nanjing (urNJ, west YRD) was similar to Pan et al. (2010), but difference existed. In addition to~~Based on observed~~ aerosol optical properties, the observed based aerosol ~~direct radiative forcing (~~DRFs~~)~~ ~~were~~ are also estimated around the world (such as: Markowicz et al., 2008; Khatri et al., 2009; Kuhlmann and Quaas, 2010; Alam et al., 2011, Zhuang et al., 2014a, and Xia et al., 2016). However, almost all of their investigations focused on the total aerosol

forcing. ~~Markowicz et al. (2008) found that the daytime surface DRF exceeded -20 W/m^2 in the Persian Gulf. Khatri et al. (2009) indicated that aerosols had strong ability to absorb solar radiation in Nagoya in summer, resulting in a positive DRF of +2.5 W/m^2 at the top of the atmosphere (TOA) and a strong negative forcing of -71.8 W/m^2 at the surface. Alam et al. (2011) found that aerosols could lead to a decrease in the TOA solar radiative flux, with a mean value of -22 W/m^2 in Karachi. In East Asia or China, Kuhlmann and Quaas (2010) indicated that shortwave radiation was reduced by about 25 W/m^2 due to the total aerosols over Qinghai Tibet Plateau.~~ For example, Xia et al. (2016) stated that regional mean aerosol DRF in China was about -16~-37 W/m^2 at the TOA and about -66 ~ -111 W/m^2 at the surface when solar zenith angle was about 60^o.

Although considerable studies on the observed columnar aerosol optical properties ~~based observations~~ have been carried out in China or even within YRD (one of the rapidest urbanization regions in China), there ~~are~~ still have gaps need to be improved ~~in~~ for the current observations ~~network in China over YRD (one of the rapidest urbanization regions in China)~~, especially in the urban areas of the region with intense human activities. In YRD or east China, most of the investigations on the aerosol optical properties were focused on the coast, lake and rural regions (Pan et al., 2010; Yu et al., 2011; Che et al., 2015a; Qi et al., 2016) of central to east YRD. And most of them only address the total aerosol optical properties (independent of modes and compositions) except Qi et al., (2016), who also made an introduction on the aerosol physical parameters and size fractional SSA in eastern coast city (Hangzhou, hereinafter short for urHZ) of YRD. There is about 300 km of urHZ away from west YRD. As implied in Zhang et al. (2012), aerosols are complicated in compositions and spatial distributions especially in fast developing regions (such as YRD). Thus, large differences of the aerosol optical and physical properties might exist to degrees among the sites within YRD. Additionally, none of

researches mentioned above have studied the aerosol DRFs. Some investigations on the columnar aerosols in west YRD (urNJ) have been carried out in Zhuang et al. (2014a), but significant issues (not considered in theirs) still need to be further addressed, such as the size fractional optical parameters and DRFs of different aerosol components, as well as the size fractional aerosol physical properties. Therefore, it's still necessary to make a more integrated investigation on the aerosol optical and physical properties, as well as their DRFs in YRD. In this study, the unaddressed issues in west or whole YRD region mentioned above will be all included based on the measurements of Cimel sun-photometer in urNJ, combined with a radiation transfer model (TUV, Madronich, 1993). Additionally, the aerosol types and mixings in the region will be further identified and discussed based on the relationships among the aerosol optical properties. Third, the observed aerosol profiles, which have not been considered before in YRD, are further used and discussed here to calculate the aerosol DRFs. It believes that the results here would be advantageous ~~To fill the gaps and~~ to ~~better~~ further understand the characteristics of aerosols~~optical properties and DRF~~ over ~~urban areas in YRD~~east region of China. Also, they are helpful to improve the model performance on the aerosol and its climate effects in relevant regions. Because, first of all, the observed aerosol parameters could be used for data assimilation to obtain more accurate inputs (including initial conditions and air pollutant emissions) of the model (Jiang et al., 2013 and Peng et al., 2017). Second, a more precise aerosol refractive index and size distribution used in numerical models would yield a more reasonable aerosol loadings and DRFs (Ma et al., 2017). Third, both the aerosol optical properties and DRFs could be used to validate the simulations.~~, we investigate the aerosol optical and physical properties observed by Cimel sun photometer (CE-318, Holben et al., 1998), as well as the aerosol direct radiative forcing calculated with a radiation transfer model TUV (Madronich, 1993) combined with observed aerosol profiles and~~

~~surface albedo in Nanjing. The aerosol optical properties include: 1). the optical depths of the total, absorbing and scattering aerosols (AOD, AAOD, SAOD, respectively) and their corresponding values in fine and coarse modes (FAOD, FAAOD, FSAOD, CAOD, CAAOD, CSAOD, respectively), 2). the Ångström exponents of the total, absorbing and scattering aerosols (AE, AAE, SAE, respectively) as well as their corresponding values in fine and coarse modes (FAE, FAAE, FSAE, CAE, CAAE, CSAE, respectively), 3). single scattering albedo of the total, fine and coarse aerosols (SSA, FSSA, CSSA) and 4). refractive indexes of the aerosols. The aerosol physical properties include: 1). the volume size distributions of the aerosols, 2). The aerosol effective and mean radius as well as their volume concentrations in all, fine, and coarse modes (R_{eff}, FR_{eff}, CR_{eff}, R_{mn}, FR_{mn}, CR_{mn}, Vol, FVol, CVol, respectively).~~

The method is described in Section 2. Results and discussions are presented in Section 3, followed by Conclusions in Section 4.

2 Methodologies

2.1 Sampling station and instruments

The observation site (Urban Environmental Monitoring Station of Nanjing University) is located in the ~~Gulou district,~~ downtown area of Nanjing City (hereinafter short for urNJ, 32.05° N, 118.78° E), west YRD. It is built on the roof of a 79.3 m-tall building, around which there ~~are~~ almost have no higher obstacles~~buildings~~ and no industrial pollution sources within a 30 km radius but there are several main roads with apparent traffic pollutions. Detailed information of the site ~~The sketch map of the site (not shown) and the corresponding climatic features are~~is available in ~~Figure 1 of~~ Zhu et al.

(2012).

The columnar aerosol optical properties and physical characters at the site were ~~observed~~ from measurements ~~using~~ of the Cimel sun photometer (CE-318, Holben et al., 1998) during the period from Apr 2011 to Feb 2014. Routine maintains and calibrations were made during the observation period. Due to the malfunctions of the instrument and the problems of data transmission, the data from May to Sep 2012 and from Aug to Dec 2013 are invalid and excluded. The wavelength dependent optical depth (AOD) and Ångström exponents (AE) of the total aerosols were directly measured by CE-318, while the following variables ~~are derived using the DOBVIC algorithm (Dubovik et al., 2000; 2006)~~, including the aerosol size distributions, fractionated~~mode dependent~~ (fine and coarse) aerosol effective radius (R_{eff}), mean radius (R_{mn}), volume concentrations (Vol), wavelength dependent size fractional ~~aerosol~~ optical depth ~~in fine (FAOD) and coarse (CAOD) modes~~ of the scattering, absorbing and total aerosols, aerosol single scattering albedo (SSA) ~~in different modes (fine and coarse), absorbing and scattering aerosol optical properties in different modes~~, as well as wavelength dependent refractive indices, are derived from the DOBVIC algorithm Version 2 (Dubovik et al., 2000; 2006). ~~The~~ This ~~DOBVIC~~ algorithm has been widely used by the Aerosol Robotic Network (AERONET) and the China Aerosol Remote Sensing Network (CARSNET) and~~.~~ the products have been used globally as introduced in Introduction due to their high accuracies. The errors for AOD, absorption AOD (AAOD), SSA is 0.01, 0.01 and 0.03, respectively (Yu et al., 2011; Li et al., 2015c). The errors of the fine and coarse aerosol SSA is 0.037 and 0.085, respectively (Xu, 2015). The error of the refractive index is 0.04 for real part and 0.0025-0.0042 for imaginary part (Yu et al., 2011). And the error of the volume size distribution is less than 10% in peak regions while about 35% in valley region or interval region between fine and coarse modes (Yu et al., 2011). Detailed descriptions on CE-318 and the

corresponding observations in CARSNET are available in Li et al. (2015a) and Che et al. (2015a). For comparison, 550 nm AODs and SSAs are calculated based on given AODs at other wavelengths and AEs (Angstrom. 1929):

$$AOD_{550nm} = AOD_{440nm} \times (\frac{550_{nm}}{440_{nm}})^{-AE_{440/870nm}} \quad (1)$$

$$AAOD_{550nm} = AAOD_{440nm} \times (\frac{550_{nm}}{440_{nm}})^{-AAE_{440/870nm}} \quad (2)$$

$$SSA_{550nm} = \frac{AOD_{550nm} - AAOD_{550nm}}{AOD_{550nm}} \quad . \quad (3)$$

To make a further comparison, the concurrent observations of surface total aerosol absorption coefficient (AAC) and Ångström exponents (AAE) measured by a 7-channel Aethalometer (model AE-31, Magee Scientific, USA, Hansen et al., 1984; Weingartner et al., 2003 and Arnott et al., 2005) are used. Detailed calculation and correction of AAC at the site could be found in Zhuang et al. (2015). In addition, monthly mean optical depth (AOD) and Ångström exponent (AE) of the total aerosols from satellite of Moderate Resolution Imaging Spectroradiometer (MODIS) were used to assist the analysis.

Based on observed wavelength dependent aerosol optical properties, the aerosol direct radiative forcing (DRF) in ~~Nanjing~~ urNJ is investigated using a radiation transfer model TUV (Madronich, 1993). Only clear sky DRFs are addressed here because almost all of the measurements are carried out in free sky condition. The solar component of the radiative transfer scheme in TUV follows the δ-Eddington approximation. In addition to the aerosol optical properties, surface alebdo (Palancar and Toselli, 2004) and the aerosol vertical profiles (Forster et al., 2007) might also have significant influences on DRF. Thus, the wavelength dependent surface albedo from MODIS, the annual and seasonal mean aerosol profiles from Cloud-Aerosol Lidar and Infrared Pathfinder Satellite Observations (CALIPSO) and

Polarization-Raman Lidar in Nanjing would be included when assessing the aerosol DRF ~~in clear sky condition~~. The aerosol DRF in this study is defined as the difference in net shortwave radiative fluxes between including and excluding aerosol effects at the TOA ~~or~~ and ~~at the~~ surface. Gas absorptions in the atmosphere were set to be constant. The scattering aerosol's SSA was set to 0.9999 (similar to sulfate or nitrate, Li et al., 2015b) when calculating its DRF. DRF of the absorbing aerosols is derived from the differences between the total and the scattering aerosol DRFs.

3 Results and discussions

3.1 Optical properties of the aerosols

In this section, 550 nm optical depth, single scattering albedo and 440 nm refractive indices of the aerosols are discussed as representatives for the temporal variations and frequency distributions of these three kinds of the aerosol optical ~~properties~~parameters. In addition to the ~~total~~ whole mode aerosols, the size fractional ~~both (~~fine and coarse ones~~), as well as both~~ aerosol optical properties of different components (scattering and absorbing aerosols) are also discussed in this section. Therefore, there are altogether nine types of aerosols, including the total aerosols, total fine aerosols, total coarse aerosols, scattering aerosols, fine scattering aerosols, coarse scattering aerosols, absorbing aerosols, fine absorbing aerosols, and coarse absorbing aerosols.

Table 1 ~~summaries~~summary the statistics of the aerosol optical properties during the study period in ~~Nanjing~~urNJ. The mean~~s for the total, scattering and absorbing aerosols'~~ 550 nm optical depth (AOD) ~~at 550 nm, averaged for the entire period,~~of the total aerosols is~~are~~ 0.65, ~~0.61, and 0.04, respectively. AAOD only accounts for about 6% to the totals~~and the scattering aerosols account for as large as about 94%. Fine mode aerosol AODs (FAOD, FSAOD and FAAOD) accounts for 81.53%, 81.97% and

56.09% of the total AOD, scattering AOD (SAOD) and absorbing AOD (AAOD) in this wavelength, respectively, implying that coarse aerosols is more absorbing than the fine ones. 440/870 nm AE of the total, scattering and absorbing aerosols are about 1.20, 1.19, and 1.32, respectively. Fine aerosols have much larger AEs, ~~. FAE, FSAE and FAAE are about~~ 0.4~~-~~0.5~~, 0.5 and 0.4~~ larger than ~~AE, SAE and AAE, respectively~~the total aerosols. Overall, the absorbing aerosols have smaller sizes than the scattering ones in all modes, especially in coarse mode, which is consistent with the results of the surface aerosols at the site (Zhuang et al., 2017). Annual mean 470/660 AAE (from AE-31) and 450/635 nm SAE (from Nephelometer Model Aurora 3000) of the near surface aerosols are 1.58 and 1.32, respectively, at the site during the period from March 2014 to Feb 2016 (Zhuang et al., 2017). The mean 550 nm SSAs are 0.93, 0.95 and 0.82 for the total, fine and coarse aerosols, respectively, further implying that the coarse aerosols have different compositions and have much stronger ability to absorb solar short wave radiation than the fine aerosols. Comparisons also indicate that surface aerosol (SSA=0.9 in Zhuang et al., 2017) is a little more absorption than the columnar aerosols in urNJ. Annual mean surface SSA at 550 nm for the total aerosols is little smaller (0.9) than the column one. The mean 440 nm refractive index is about 1.44+0.0084i. The table also implies that west YRD could suffer very serious particle pollutions.

Table 1

3.1.1 Seasonal variations of the aerosol optical properties

Figure 1 presents the monthly variations of 550 nm AOD (a), SAOD (b) and AAOD (c) as well as the contributions of their fine or coarse mode to the corresponding totals. Temporal variations of the total aerosol AOD is consistent with SAOD due to significantly large ratio of SAOD/AOD. AODs are

all considerably high in winter due to a more intense emission of the trace gases and particles (~~According to~~ Zhang et al., ~~(~~2009)~~,~~ ~~anthropogenic emissions of trace gases and aerosols have substantially seasonal variations, low in summer but high in colder seasons especially in winter. Therefore, AODs, including the total, scattering and absorbing ones, are considerably large in winter.~~ However, a long distance transported ~~due to the effects of~~ dust aerosols from north China in spring and high efficiencies of moisture absorption and scattering aerosol chemical transformation in summer (Li et al., 2015a~~),~~) also lead to high AODs ~~are also large~~ in these two seasons. ~~Additionally, gas to particle transformation might be more efficient in summer, which somewhat contribute to larger SAOD or FSAOD in this season. Overall, lower AODs are all found in fall for the total, scattering and absorbing aerosols.~~ Therefore, dust episodes, relative humidity (RH) and chemical processes weaken the seasonal variation of total AOD purely induced by the emissions in urNJ, west YRD. ~~tradeoff among anthropogenic emissions, dust aerosols, and relative humidity somewhat weakens the seasonal variations of the all-mode aerosol optical depth, including AOD, SAOD and AAOD.~~ Instead, these processes prominent the AOD seasonality of different aerosol types in different size segments. ~~However, the seasonalities of fine and coarse aerosol AODs are very different from and much stronger than the total mode aerosols.~~ The largest AODs appear in spring for coarse scattering and absorbing aerosols ~~(for both scattering and absorbing ones)~~ while ~~the largest AODs~~in summer for the fine ~~aerosols are found in summer~~ ones in urNJ. ~~The coarse aerosol AODs are lowest in summer or fall while for fine aerosol AODs, the minimum appears in spring.~~ The figure also implies that the scattering aerosols might have different size distribution from the absorbing aerosols. The fine mode fraction rate is 0.83 (peaking at 0.97) for scattering aerosol while 0.56 (peaking at 0.83) for absorbing aerosol.~~Owing to this, contributions of fine or coarse aerosol AODs to the totals are different among~~

~~different months. The peaks of FAOD/AOD, FSAOD/SAOD, and FAAOD/AAOD appear in August, with a value of 0.96, 0.97, and 0.83, respectively, while the largest values of CAOD/AOD, CSAOD/SAOD, and CAAOD/AAOD appear in April, being 0.35, 0.32, and 0.64, respectively.~~ In other words, the fine aerosols have different compositions from the coarse ones. ~~The figure further suggests that the scattering or total aerosols are mostly composed by the fine particles (>80%) while the absorbing aerosols are composed, at the same level, by both fine (56%) and coarse (44%) particles in column atmosphere in Nanjing, reflecting more absorbing of the coarse aerosol than the fine one.~~

Figure 1

The aerosol Ångström exponents also have substantially seasonal variations, especially for the absorbing aerosols as illustrated in Figure 2~~, showing monthly AE, FAE, CAE, SAE, FSAE, CSAE, AAE, FAAE, and CAAE at 440/870 nm. Similar to AODs,~~. ~~the seasonality of the total aerosol AEs is similar to that for the scattering aerosols. However, the seasonalities of the total and scattering aerosols is less profound than those of absorbing aerosols.~~ For each component (scattering or absorbing one), the seasonal variations of its fine and coarse AEs are well agree with each other, ~~Both fine and coarse aerosol AEs are~~all being close to zero line in summer ~~for scattering and absorbing aerosols~~ possibly due to the effects of high relative humidity ~~in this season~~ (Zhuang et al., 2014a)~~, implying that both fine and coarse mode aerosols have larger sizes in summer than in the other seasons~~. ~~The monthly variations of FAAE and CAAE are similar to each other, small in summer and large in spring and winter, although their magnitudes are different (Figure 3). However, FSAE and CSAE are strongly anti-correlated.~~ The whole mode AE of each aerosol type is determined by the both variations of AE in

each mode and fine mode fraction. Therefore, the smallest ~~seasonal variation of the total absorbing aerosol~~ AE ~~(AAE), to some degree, agrees with that of FAAE or CAAE; its minimum~~ appears in summer (0.74 in July) for the total absorbing aerosols while ~~. However, CAAOD accounts for the most to AAOD in spring, AAE values are smaller, closer to CAAE's in this season than in fall and winter. The seasonality of SAE is different from both FSAE's and CSAE's; it is also different from AAE's. Under the combined effect of FSAE and CSAE, SAE minimum appears~~ in spring (0.94 in Mar) for the total scattering aerosols~~while the larger ones are found in summer and fall~~. ~~Similar to AAE but more, the curve of SAE would move toward the sides of CSAE in spring while toward FSAE side in summer because the peaks of CSAOD/SAOD and FSAOD/SAOD appears in spring times and in summer times, respectively as shown in Figure 1.~~ Similarly, the total aerosol AE is determined by the both variations of each aerosol type's AE and fraction rate of the scattering (or absorbing) aerosol to the totals. Similar to AOD, the seasonality of the total aerosol AEs is more consistent with that of the scattering aerosols. The figure also indicates that the ~~coarse~~ scattering aerosols have much larger sizes ~~(negative values of CSAE)~~ than the ~~coarse~~ absorbing aerosols, especially in coarse mode. ~~suggesting that the CSAE might have much greater influence on the total SAE than CAAE on the total AAE, although the ratio of CSAOD/SAOD is smaller than that of CAAOD/AAOD.~~ Further comparison indicates that t~~T~~he seasonal variations of columnar SAE and AAE are consistent with the ones of surface SAE and AAE (results not shown here) at the site.

Figure 2

In addition to AOD and AE, monthly variations of the aerosol single scattering albedo (SSA) and

refractive indices are also investigated as shown in Figure 3~~, which shows the monthly variations of the all, fine and coarse aerosol SSA at 550 nm and the total aerosol refractive indices at 440 nm~~. SSA is affected by both scattering and absorbing aerosols, as well as their relative contributions. The fine particles are much more scattering than the coarse aerosols. ~~Furthermore~~However, ~~CSSA~~ the coarse aerosol SSA has more significant seasonality ~~than FSSA~~. ~~The total aerosol single scattering albedo, i.e., SSA, is somewhere in between FSSA and CSSA depending on the ratios of FAOD to AOD.~~ Overall, both FSSA and CSSA are relative smaller in summer than in the other seasons although they are considerable large in August 2011, implying that the two types of aerosols in summer are more absorbing than in the other seasons. The total aerosol SSA is somewhere in between FSSA and CSSA depending on the ratios of FAOD to AOD and it has ~~However, SSA has a~~ different seasonal variation from FSSA or CSSA. SSA is the smallest in spring ~~Due~~ due to the largest contribution of coarse aerosols ~~in spring, SSA is the smallest in the season~~. The aerosol refractive indices also show substantial seasonality. The real part is large in spring but small in summer, which is similar to what was observed in Taihu Lake in ~~the middle of~~central YRD (Yu et al. 2011). The imaginary parts show relatively weaker seasonal variations than the real parts.

Figure 3

Table 2 summarizes the abovementioned seasonal means with the corresponding standard deviations for ~~all~~ the all aerosol optical properties ~~in the four seasons~~. It provides more quantitative variations of the aerosol optical properties compared with the figures above. Seasonal mean 550 nm AOD, SAOD and AAOD vary from 0.59 in fall to 0.75 in summer, from 0.55 in fall to 0.70 in summer,

and from 0.037 in fall to 0.050 in spring, respectively. CAOD, CSAOD, CAAOD account for the majority of AOD, SAOD and AAOD in spring, with the ratios of 30.1%, 27.9%, and 58.1%, respectively. FAOD, FSAOD, FAAOD account for the majority of AOD, SAOD and AAOD in summer, with the ratios of 90.5%, 91.2% and 70.2%, respectively. As discussed above, the seasonal variations of the total mode aerosol AEs and SSA are different from the ones in each mode ~~of fine or coarse aerosol AEs and SSA, respectively.~~ The seasonal mean 440/870 nm ~~AE,~~ SAE and AAE vary from ~~0.99 in spring to 1.37 in fall, from~~ 0.98 in spring to 1.38 in fall, and from 0.78 in summer to 1.50 in winter. Seasonal mean ~~SSA,~~ FSSA and CSSA vary ~~from 0.920 in spring to 0.938 in winter,~~ from 0.940 in summer to 0.956 in ~~winter,~~winter and from 0.787 in summer to 0.834 in spring, respectively. The real part of the aerosol refractive index has relatively stronger seasonality than the imaginary part. Their largest values are all found in spring. ~~Seasonal mean real and imaginary parts range from 1.41 in summer to 1.46 in spring and from 0.0080 in fall to 0.0084 in spring.~~ Comparisons indicate that t~~T~~he seasonal variation of the optical properties ~~AOD~~ is highly inhomogeneous spatially ~~even~~ within ~~the same region such as in~~ YRD. As indicated in Che et al. (2015a) and Qi et al. (2016), the largest AOD was found in spring while the lowest one appeared in summer in ~~Hangzhou~~urHZ, another city in eastern coast ~~east~~of YRD. In Taihu Lake, a rural site in central YRD, the lowest AOD appeared in winter (Pan et al., 2010; Yu et al., 2011). Additionally, the aerosols are the most absorbing in winter in central regions of YRD (Taihu Lake and urHZ) and their SSA are as small as 0.88 (Yu et al., 2011 and Qi et al., 2016). Aerosols in west YRD (urNJ) are more scattering than theirs and the smallest SSA appears in spring during the sampling periods. ~~The aerosols are more absorbing in winter (0.88) in Taihu Lake (Yu et al., 2011) than in spring in urban Nanjing here (0.92).~~ Nevertheless~~However~~, AE~~s~~ variations are more consistency with each other among these sites, being smallest in spring and largest

398 in fall.

399 Table 2

400

401 **3.1.2 Frequencies of the aerosol optical properties**

402 All AODs and SSAs follow a near lognormal pattern and almost all of the AE and refractive
403 indices follow a unimodal pattern (Figure 4). The ranges around their means dominated, accounting for
404 at least 60% to their total data samples during the entire study period. Similar to the temporal variation,
405 frequency distributions ~~In addition to the seasonal variations, frequency distributions of the~~
406 ~~abovementioned aerosol optical properties are also investigated. Figure 4 presents the frequencies of~~
407 ~~550 nm AOD, FAOD, CAOD, SAOD, FSAOD, CSAOD, AAOD, FAAOD and CAAOD in Nanjing~~
408 ~~during the entire study period. All AODs follow a near lognormal pattern. The curves~~ of the total
409 aerosols (~~Fig. 4a~~not shown) are also highly similar to the ones of scattering aerosols ~~(Fig b) ,~~ ~~at the~~
410 ~~same bandings,~~ in both fine and coarse modes. ~~The peaks of the frequency curves, all exceeding 30%,~~
411 ~~appear at the values between 0.3 and 0.5, 0.2 and 0.4, 0.04 and 0.08 for all and scattering aerosol AODs~~
412 ~~in all, fine and coarse modes, respectively. They appear at the values between 0.005 and 0.02, 0.005~~
413 ~~and 0.015, 0.005 and 0.01 for AAOD, FAAOD and CAAOD, respectively. The dominant ranges are~~
414 ~~from 0.3 to 0.9 for SAOD (AOD), 0.2 to 0.8 for FSAOD (SAOD) and 0.04 to 0.16 for CSAOD~~
415 ~~(CAOD), accounting for more than 83% (82%), 83% (82%), and 63% (67%), respectively, of the total~~
416 ~~data samples during the entire period. The dominating ranges are from 0.005 to 0.06 for AAOD, 0.005~~
417 ~~to 0.05 for FAAOD and 0.005 to 0.03 for CAAOD, accounting for more than 75%, 82% and 71%,~~
418 ~~respectively, of the total data samples during the entire period. The curves vary in different seasons (not~~
419 ~~shown here), shifting left ward in low AOD seasons and right ward in high AOD seasons as suggested~~

~~by Zhuang et al. (2015). In summer, the curves might even have two peaks for the scattering or total aerosols, which is similar to the observations in Taihu Lake (Yu et al., 2011). The frequency curve of the total AOD is much closer to that of fine AOD for scattering aerosols than for absorbing aerosols because FSAOD accounts for more than 82% of SAOD while FAAOD only accounts for 56% of AAOD.~~

~~Figure 4~~

~~Due to the large ratio of the scattering aerosols to the total aerosols, the frequency of the total aerosol AEs resembles more that of the scattering aerosol AEs (Figures 5a and 5b). Almost all the AE frequencies follow a unimodal pattern, less sharply than those of the AODs in Figure 4. The dominant ranges are from 0.8 to 1.6 for SAE (AE), 1.3 to 2.1 for FSAE (FSAE) and -0.48 to -0.24 for CSAE (-0.24 to -0.12 for CAE), accounting for more than 81% (83%), 83% (83%) and 82% (75%), respectively, of the total data samples during the entire period. The dominant ranges are from 0.8 to 1.8 for AAE, 1.1 to 2.1 for FAAE and 0.6 to 1.6 for CAAE, accounting for more than 74%, 67% and 69%, respectively, of the total data samples during the entire period, implying a gentler curve of AAE than SAE.~~ The frequencies of the absorbing aerosol AEs ~~in different modes~~ are different from ~~those of~~ the scattering ~~aerosols~~ ones~~(Figure 5b and 5c)~~, so is FAAE and CAAE. The occurrences of smaller CAAE are relatively high. ~~The values below 0.6 for CAAE account for more than 20% of the total data samples. In addition~~However, the ~~occurrences of the~~ large FAAE ~~and AAE~~ exceeding 2.5 ~~and 2.2 reach~~ also has contributions (more than 5.4%) ~~and 11%, respectively, implying again that the absorbing aerosols in fine mode have a few parts of finer particles~~. Both fine and coarse absorbing aerosols have

much smaller sizes than the scattering aerosols at the same modes. ~~The frequencies of AEs also have substantial seasonality (not shown here). Comparing with the annual frequency of SAE, the peak of the frequency shifts left-ward in spring, from 0.8 to 1.0, but shift right-ward in fall, from 1.4 to 1.6. The frequency of AAE has a left-ward shift in summer compared to the annual one, peaking at AAE values between 0.6 and 0.8.~~

~~Figure 5~~

~~SSAs also follow a near lognormal pattern (Figure 6a).~~ Frequency distribution of SSA also implies that t~~T~~he coarse aerosols are more absorbing than the fine aerosols ~~(Table 1 and Figure 3)~~. Consequently, the frequencies of SSAs peak~~s between 0.91 and 0.93,~~ between 0.95 and 0.97, and between 0.80 and 0.84 for the ~~all,~~ fine~~,~~ and coarse mode aerosols, respectively, in ~~Nanjing~~ urNJ during the study period. ~~The dominant frequency appears from 0.89 to 0.97 for SSA, from 0.91 to 0.99 for FSSA, and from 0.72 to 0.92 for CSSA, accounting for more than 75%, 87% and 78%, respectively, of the total data samples during the entire study period.~~ Fine aerosol SSAs concentrates more in a narrow range (from 0.89 to 0.99) than CSSA (from 0.64 to 0.96). ~~Both real and imaginary parts of the aerosol refractive index follow a unimodal pattern and they are fairly similar to each other (Figure 6b).~~ For the refractive index, t~~T~~he frequencies peak between 1.39 and 1.42, and between 0.007 and 0.009 for the real and imaginary parts, respectively, in ~~Nanjing~~ urNJ during the study period. ~~The prevailing frequency ranges from 1.36 to 1.54 for the real part and from 0.003 to 0.013 for the imaginary, accounting for more than 76% and 70% of the total data samples, respectively.~~

The frequency patterns of the aerosol optical properties also have substantial seasonality (not

shown here). Overall, the curves would shift left-ward in low value seasons and right-ward in high value seasons. In summer, the AOD curves might even have two peaks for the scattering or total aerosols, which are similar to the observations in Taihu Lake (Yu et al., 2011). For SAE, the peak shifts left-ward in spring by 0.2, but right-ward in fall by 0.2. For SSA, ~~The seasonality of SSA frequency (not shown) indicates that~~ both fine and coarse aerosol SSA frequencies have a left-ward shift in summer compared to the annual one, which is opposite to the frequency of the total SSA because the fine aerosol AODs dominate, accounting for about 91% of the totals. The real part frequency in spring has a significant right-ward shift compared to that in the entire study period, peaking between 1.46 and 1.50 (not shown). The imaginary part frequency in winter has a significant left-ward shift compared to that in the study period, peaking between 0.001 and 0.003 (not shown).

~~Figure 6~~

~~——~~

3.1.3 Comparisons with MODIS AOD, AE and surface aerosols

AOD and AE observed by CE-318 are in reasonable agreement with those from MODIS in seasonal variation and magnitude (Figure ~~7~~5). The linear correlation coefficients are 0.75 and 0.86 between CE-318 AOD and MODIS AOD and between CE-318 AE and MODIS AE, respectively. AOD at 550 nm from MODIS is larger than from CE-318, with an ~~averaged~~average value of 0.82 during the study period. The mean AE at 412/470 nm is about 1.43. The standard deviations of the AOD and AE are much larger from CE-318 than from MODIS possibly due to a higher temporal resolution of CE-318 observations.

Figure ~~7~~5

The columnar AAOD and AAE from CE-318 are fairly related to the surface aerosol absorption coefficient (AAC) and AAE from AE-31 (Figure ~~8~~6). However, the relationship between AAOD and AAC or between column and surface AAEs is worse than that between CE-318's and MODIS'. Although surface aerosols could be affected by transport, it is mainly from local and regional emissions and its loadings are highly related to the degree of the boundary layer development. As suggested by Zhuang et al. (2014b and 2015), surface aerosol loadings are considerably low in afternoon and summer times when the boundary layer are well developed. The columnar AAOD could additionally be affected by the ~~upper aerosol~~ emissions and transportations in the upper atmosphere and it is less affected by the boundary height compared with the surface AAC, thus contributing a relatively worse relationship between AAOD and AAC. The surface AAE is more concentrated in a narrow range and it is larger (1.6) than that from CE-318, implying that the surface absorbing aerosols are finer ~~thus~~ and fresher. The linear correlation coefficients are 0.39 and 0.41 between AAOD and AAC and between columnar and surface AAEs, which is slightly worse than those between FAAOD and AAC (0.46) and between columnar FAAE and surface AAE (0.47).

Figure ~~8~~6

3.1.4 Briefly discussions

——Ground based observed aerosols have much higher temporal resolutions compared with satellite retrievals. The observed columnar optical properties could make up the deficiency of surface

aerosol data on one hand, and make us better understand the characteristics of the aerosols on the other hand. Additionally, they might be useful for improving the model performances on the aerosols and their radiative effects in YRD or east China. The observed aerosol parameters could be used for data assimilation, which can produce more accurate initial conditions of the model and variations of the aerosol emissions (Jiang et al., 2013 and Peng et al., 2017). The data set of the optical properties in most of the climate or air quality models are frequently from a given refractive index which is homogeneous in time and space. Therefore, a more precise aerosol refractive index used in numerical models would yield a more reasonable aerosol optical properties and radiative forcing in observed regions and around. Further, the observed aerosol optical properties could be also used to validate the simulations.

As mentioned in Introduction, m~~M~~ost studies on the aerosol optical properties in China mainly focus on AOD and AE of the total aerosols in short term (i.e., episodes, Che et al., 2013; Zheng et al., 2016; Che et al., 2015b). Studies on annual (Yu et al., 2011) and decadal (Che et al., 2015a) scales have been carried out in recent years based on CE-318 measurements. Che et al. (2015a) indicated that long tern averages of the total aerosol ~~optical depth~~AOD at 440 nm and ~~Ångström exponent~~AE at 440/870 nm in urban areas were about 0.75 and 1.05 in north China, 0.98 and 1.09 in Sichuan Basin, 0.78 and 1.36 in Pearl River Delta region (PRD), 0.65 and 1.0 in northeast China, 0.66 and 89 in northwest China, 0.92 and 1.0 in central China, 0.9 and 1.25 in coastal areas of YRD. The mean AOD at 440 nm in ~~urban Nanjing~~urNJ ~~averaged over the study period is about 0.84, which~~ is larger (0.84) than that in northern China~~, northwest China, northeast China,~~ and PRD but smaller than that in coastal cities of YRD~~ and about the same as the one in HeFei (0.84)~~. Aerosols in north~~west~~ern and central China~~, central China, north China~~ have larger sizes (smaller AE) than those in ~~Nanjing~~west YRD.~~ AE in the~~

~~cities and at rural areas within YRD is at a similar magnitude.~~ Che et al. (2015a) further suggested that the aerosols in urban areas likely had larger AODs and AEs than those in mountain and desert areas, so did in ~~Nanjing~~urNJ. Qi et al. (2016) presents that the aerosol single scattering albedo at 440 nm in urHZ~~Hangzhou, east YRD~~ is about 0.90, 0.92 and 0.70 for the total, fine and coarse aerosols, respectively, also implying that the coarse aerosols are more absorbing than the fine ones. Our measurements show similar results to ~~Qi et al. (2016) for Hangzhou~~theirs. However, aerosols in ~~Nanjing~~ urNJ are more scattering than in ~~Hangzhou~~ urHZ in both fine and coarse modes, revealing inhomogeneous distributions of the aerosol compositions in YRD. Although some studies on the columnar aerosol optical properties based observations have been carried out in YRD (Pan et al., 2010; Yu et al., 2011; Zhuang et al., 2014a; Che et al., 2015a, Qi et al., 2016), study here further fill the gaps of the current observations. Based on authors previous research (Zhuang et al., 2014a), a more comprehensive and systematic analysis on the fractionated optical properties of different aerosols types are additionally carried out here. The results would be advantageous to further understand the aerosols over east China.

3.2 Physical properties of the aerosols

In addition to the optical properties, the aerosol physical properties including volume size distributions, mode dependent sizes (radius) and volume concentrations are also retrieved. Figure ~~9~~ 7 shows the volume size distributions of the aerosols in different seasons (Figure ~~9a~~7a) and in different AOD (or polluted) levels (Figure ~~9b~~7b) in ~~Nanjing~~urNJ. The figure shows that a~~A~~erosols in ~~Nanjing~~ urNJ have a typical bimodal structure in volume size distribution in all seasons, presenting a two-mode lognormal distribution: fine ~~mode~~ (radius < 0.6 μm) and coarse mode (radius > 0.6 μm). Their annual

peaks appear at the radius of 0.148 μm in fine mode and 2.94 μm in coarse mode. Similar to the aerosol optical properties, aerosol volume size distribution also has substantial seasonality. Dust episodes lead to ~~T~~the peak value in spring ~~is~~ being much ~~lower~~ smaller in fine mode ~~and higher~~than in coarse mode, which is opposite to ~~than~~ that in the other seasons (especially in summer). ~~due to the effect of dusts which results in a left-ward shift in the distribution in fine mode.~~ Therefore, the mean radius of the aerosols increases significantly in spring due to a high proportion of coarse particles, leading to a smaller AE as discussed in precious sections. In summer, the curve has a right-ward shift, showing ~~an~~ a ~~increase~~ larger aerosol size in both fine and coarse ~~aerosol sizes~~modes due to high hygroscopic growth efficiency~~levels of moisture in the season~~. The fine particles dominate in summer and result in large AE, opposite to what is in spring. ~~In Nanjing, t~~The aerosol volume size distribution varies with different AOD values (Figure ~~9b~~7b) in urNJ. Overall, the peak~~s~~ value ~~likely~~has a substantial ~~shift~~ right-ward shift with increasing AOD for fine aerosols ~~but~~while a slightly left-ward shift for coarse aerosols~~.~~, implying that the growth of the fine aerosols is advantageous to enhance the aerosol radiative effect. In urNJ, both fine and coarse particles basically have the same levels ~~The peaks are at the radii of 0.113 and 3.857 μm~~ when AOD is below ~0.2~~ 8. And the fine aerosols begin to dominate more ~~and at 0.194 and 2.94 μm~~ when AOD exceeds 0.8~~1.4~~. ~~Additionally, AOD show a positive dependence on the volume concentrations of both fine and coarse aerosols. The AOD in Nanjing could be evenly affected by both fine and coarse aerosols when AOD is considerably large or relatively small. High levels of AOD (>1.4) are attributed to the coarse aerosols in spring and to the fine aerosols in summer. AOD values ranging from 1.0 to 1.4 is more resulted from the fine particles.~~ The results here are rather consistent with the ones in Yu et al. (2011), Qi et al. (2016), and Zheng et al. (2016). However, the figure here further reflects that both fine and coarse particles themselves could cause very serious haze pollutions in YRD,

leading to considerably high peaking values in both fine and coarse modes being found. This has not been observed in previous publications. The aerosol size distributions here are also very useful for optimizing numerical models. A more precise aerosol size distribution would make the models more accurate in describing the aerosol transportation, deposition as well as its radiative effects (Ma et al., 2017) in YRD or east China.

Figure ~~9~~7

To further investigate the physical features, t~~T~~he seasonal variations ~~in~~ of the aerosol effective and mean radius, ~~and~~ as well as volume concentrations in ~~Nanjing~~ urNJ are further presented in Figure ~~10~~8. The mean effective radius ~~are~~, which is generally smaller than the mean one in all modes, is about 0.34, 0.16, and 2.18 μm for the total, fine and coarse aerosols, respectively, during the study period. It additionally reflects that the aerosols in urNJ are dominated by the fine particles as discussed previously. ~~The mean averaged radius are about 0.80, 0.19, and 2.67 μm for the total, fine and coarse aerosols, respectively.~~ The ~~The seasonal variation of the aerosol effective~~ seasonal variations of the radiuses have a good anti-correlation to the one of AEs (Figure 2). ~~resembles that of the mean radius in all the modes.~~ Both fine and coarse aerosol radius are larger in summer than in the other seasons due to the moisture absorption growth of the aerosols. ~~With seasonal variations in the proportion of fine or coarse aerosols in the total~~However, the total aerosol radius ~~of the total aerosols are~~is much larger in spring ~~than in the other seasons~~due to a larger coarse fraction. ~~The seasonal variations of the radius in all modes anti-correlate well with the corresponding aerosol AEs as shown in Figure 2.~~ Different from the radius, the seasonal variations of the volume concentrations between fine and coarse aerosols are

different, peaking in spring for coarse aerosol while in summer for fine aerosol. ~~The mean volume concentrations are 0.24, 0.11 and 0.13 μm^3/cm^3 for the total, fine and coarse aerosols during the study period. Overall,~~ Although both the fine and coarse aerosols have the same volume levels~~evenly contribute to the total aerosol volume~~ in ~~Nanjing~~urNJ annually, their contributions to the total aerosol volumes vary significantly with seasons.~~similar to what is found in Hangzhou (Qi et al., 2016). The coarse aerosols contribute slightly more to the total aerosol volume concentrations because of its high proportions in spring (Figure 10b). The seasonality of the volume concentrations in fine and coarse aerosols are different, although the seasonality of their radius are similar to each other, because the volume also depends on the concentrations of the aerosols. The highest volume concentrations appear in spring for the coarse aerosols and in summer the for fine aerosols. As expected,~~ Tthe coarse aerosol directly leads to the largest~~seasonal variation of the total aerosol volume is affected by both fine and coarse aerosols~~volume peaking in spring for the total aerosols.

Figure ~~10~~8

3.3 Aerosol classification based on its optical properties

The aerosol ~~types~~clusters, to a certain degree, could be identified based on the relationships between SSA at 491 nm and AE at 491/870 nm, between real refractive index (RRI) at 670 nm and AE at 491/870 nm, as well as between SSA differences (dSSA=SSA_{870nm}-SSA_{491nm}) and AE at 491/870 nm as presented in ~~(~~Russell et al.~~,~~ (2014), who ~~as shown in Figure 11. Russell et al. (2014)~~ proposed a Mahalanobis Classification based on "a priori" information for each type aerosol source (e.g.: dust, urban, biomass aerosols). Different aerosols then would mostly concentrate within the corresponding

ellipses of a two-dimensional scatter plot of SSA versus AE (or RRI versus AE, or dSSA versus AE). Based on their classification, the pure dust, polluted dust, biomass-burning, industrial urban, developing urban, marine aerosols (Figure 8 in Russell et al., 2014) all could be identified. ~~indicated that~~For example: 1. The polluted dust aerosols would be mostly within the ellipses with~~have~~ smaller AE (near 1.0), relatively smaller SSA levels (0.85 to 0.95), but much larger real refractive index (1.45 to 1.55) and SSA differences (0 to 0.05) compared with other aerosols. 2. The aerosols from the developing urban generally have smaller sizes than the polluted dust (AE ranging from 1 to 1.6), but they have larger SSA (0.9 to 1.0), smaller real refractive index (1.4 to 1.5) and SSA differences (around 0). 3. The aerosols from the urban dominated by Industrial (UrbInd) or from biomass burning have the largest AE (exceeding 1.6). However, the UrbInd aerosols have much larger SSA and SSA differences while smaller real refractive index compared with biomass burning aerosols. ~~If there were two kind of aerosols having nearly identical coordinates, further information is needed.~~ Based on their classification standards, aerosols in urNJ could basically be identified as the clusters of polluted dust, developing and industrial urban kinds during the sampling period as shown in Figure 9, which further supports the analysis in previous sections (Section 3). In spring, dusts emitted from the desert regions in northern or north of China ~~the Figure 11 presents that aerosols in urban area of Nanjing~~ could be ~~effected by the long distant~~ transported ~~dust (or polluted dust) substantially in spring times~~in long distant arriving to YRD. During the transportation, trace gases or particles could be absorbed and then a heterogeneous chemical reaction occurs. And in ~~rest~~ other seasons, the aerosols are mostly from the local emissions within ~~and they belong to the developing~~ the urban areas and industrial areas around ~~aerosols~~. Although urNJ is only about 300-400 km far away from the East China Sea, its aerosols are few composed by marine or sea salt components as illustrated in Figure 9. It is a pity that the

observations missed a biomass burning event in Jun 2012 (Zhuang et al., 2014b, 2015) when the instrument was maintained. Otherwise, the figure will be more comprehensive. It's a very serious biomass burning episode, which directly results in extremely high BC surface concentrations (6-7 times to the annual means, Zhuang et al., 2014b). Analysis here might further help us to understand the aerosol sources, transformations, transports and its radiative effects in YRD. And it ~~Figure 11 would be more comprehensive if this event were captured.~~ also indicates that the Mahalanobis Classification is a very useful approach for classifying the aerosol into types, especially in the cases of shortage of data or insufficient of methods. However, the method still has a limitation. The classified ellipses have some overlaps among different aerosols clusters. In overlap regions, it's hard to further identify the aerosol into types. For example, it's not easy to distinguish the polluted dust aerosol with large AE from the urban aerosols with smaller AE. Therefore, if there were two kinds of aerosols having nearly identical coordinates, further information is needed or more effective approaches should be taken into account.

Figure ~~11~~9

In addition to the types, the aerosol mixtures/compositions could also be identified based on SSA and AAOD. Generally, dust aerosol has strong absorptions in ultraviolet (UV) band, but become non-absorbing in the visible band, leading to its ~~and biomass burning aerosol~~ SSAs increasing with wavelength monotonically. For biomass burning aerosol, its SSA would ~~increase and~~ decrease with wavelength~~, respectively~~ monotonically. Non-monotonically ~~changes~~variation in SSA with the wavelength might be due to the other type aerosol dominated mixtures as indicated by Li et al. (2015c), who then proposed two curvature parameters defined as the second derivative of the second-order

polynomial fit of SSA and wavelength and the fit of AAOD and wavelength as shown in Eq. 4 and Eq. 5 to provide additional information on the aerosol compositions.

$$\ln(SSA_\lambda) = \beta_2 \ln(\lambda)^2 + \beta_1 \ln(\lambda) + \beta_0 \quad (4)$$

$$\ln(AAOD_\lambda) = \alpha_2 \ln(\lambda)^2 + \alpha_1 \ln(\lambda) + \alpha_0 \quad (5)$$

Where, $-\beta_2$ and α_2 are the SSA Curvature and AADO Curvature, respectively. Detailed statements could be found in Li et al. (2015c). Based on these parameters, the aerosols could basically be identified as the dust dominated, black carbon (including biomass burning and urban/industrial aerosols) dominated and other mixed (peak) type aerosols, because the curvature probability (or frequency) distributions are different among different aerosol mixtures. ~~The former two type of aerosols have monotonically increase and decrease SSA spectral shapes, respectively.~~ As indicated in Li et al. (2015c), t~~T~~he SSA or AAOD Curvature is mostly concentrated at or around 0 for the BC dominated aerosol mixture, which is much smaller than that of dust dominated aerosol mixtures (0.1 for SSA Curvature and 0.5-1 for AAOD Curvature) ~~(Li et al., 2015c)~~over East Asia. Based on their method, the curvatures of SSA and AAOD are calculated and then divided into three categories according to the monotonicity of SSA. Results show that there are about 15.0%, 27.5% and 42.3% occurrences of monotonically increasing, decreasing and 670 nm peaking SSA spectrums, respectively, in urNJ. And their probability (or frequency) distributions are plotted in Figure 10. Both SSA and AAOD Curvatures have substantial seasonality, larger in colder seasons (not shown here). The figure indicates that ~~Our observations show the similar results as shown in Figure 12~~the SSA and AAOD curvature patterns are highly consistent with those in Li et al. (2015c) for the monotonic categories, which implying that there might be about 15% (mostly appearing in spring) and 27% (mostly being in fall and winter) occurrence of dust dominated and BC dominated mixing aerosols, respectively, in urNJ

during the observed period. For example, a very strong dust storm from northwest China and Mongolia (Li et al., 2015a) directly yielded mean SSA and AAOD Curvatures of 0.12 and 1.11, respectively, on 1st May 2011, which are close to the values (0.11 and 1.24, respectively) of the pure dust aerosol (Li et al., 2015c). ~~, further implying that aerosols in urban Nanjing could be effected by the long distant transported dust as indicated in Figure 11 and could also be affected by biomass burning or the industrial emissions. The results additionally suggested that there are about 15% (mostly appearing in Spring) and 27.5% (mostly being in Fall and Winter) occurrence of dust dominated and BC dominated mixing aerosols, respectively, in urban areas of Nanjing during the observed period.~~ For the rest category with non-monotonic SSA spectrum, the SSA curvature are mostly concentrated from 0.3 to 0.8, implying that dust component might not exceed 10% while the scattering species (organic carbon not included) at least accounting for 30% within the mixing particle in west YRD according to the sensitive results in Li et al. (2015c). Subsidiary data are needed if more information were going to be further identified. Results here might help us to better understand the mixings of the aerosols in urban areas of YRD. Similar to the Russell et al. (2014), Li et al. (2015c) also provides an effective approach to classify the aerosol compositions based on a single data set (such as the CE-318 retrievals).

Figure ~~12~~10

~~In May 2011, Nanjing was affected by a very strong dust storm from northwest China and Mongolia (Li et al., 2015a), the mean SSA and AAOD Curvatures in 1st May 2011 were as large as 0.12 and 1.11, respectively, which is close to the values (0.11 and 1.24, respectively) of the pure dust aerosol (Li et al., 2015c). Both SSA and AADO Curvatures have substantial seasonality, larger in~~

~~colder seasons (not shown here).~~

3.4 The direct radiative forcing of the aerosols

Basing on abovementioned wavelength dependent optical properties and combining with the observed surface albedo and aerosol profiles, the clear sky size fractional ~~total, scattering and absorbing~~ aerosol direct radiative forcing (DRF) of different components ~~in all, fine and coarse modes~~ at both the top of atmosphere (TOA) and ~~the~~ surface in ~~Nanjing~~ urNJ ~~using~~ are investigated using a radiation transfer model TUV (Madronich, 1993)~~, under clear sky condition~~. Due to lacking SSA observations of each aerosol component, t~~T~~he scattering aerosol DRF~~'s~~ ~~SSA~~ is estimated based on a given SSA value (0.9999, ~~assumed to be~~ equaling to that of sulfate or nitrate aerosol) in reference~~,~~ ~~which is about 0.9999~~ (Li et al., 2015b) ~~when assessing its DRF~~. As indicated in last section, absorbing aerosols in urNJ are always in a mixed state. Therefore, t~~T~~he absorbing aerosol DRF ~~was~~ is inappropriate to be estimated directly using the BC SSA. Here, it is derived from the difference between the total ~~aerosol~~ and scattering aerosol DRFs, which might be more representativeness ~~because of lacking the observed SSA of the mixed absorbing aerosol~~. To make comparison, the aerosol DRF~~s~~ is also calculated based on AAODs, AAEs and black carbon (BC) SSA (Li et al., 2015b) ~~is also calculated to make a comparison with the absorbing aerosol DRFs~~.

Observed aerosol profiles, which have not been used in previous investigation (e.g.: Zhuang et al., 2014a), might be important to the DRFs estimating. Figure ~~13~~ 11 shows the mean vertical aerosol profiles ~~of the aerosols~~ observed by CALIPSO (annual scale data) and Polarization-Raman Lidar (PRL, seasonal scale data) in Nanjing. To make a comparison, all profiles in the figure have been standardized to the percentage (%). Similar to AODs and AEs, the figure suggests that the ground and satellite based

aerosol profiles also exist substantial differences. The CALIPSO profile is more homogeneous than the PRL one, ~~The aerosols mainly concentrate below 4 km,~~ accounting for about 61% and 88%, respectively, ~~according to CALIPSO and Lidar, respectively, suggesting that differences exist between CALIPSO and Lidar derived profiles and the vertical aerosols from the Lidar distribute much more at the lower troposphere~~below 4 km. Due to lacking long-term measurement of PRL and the different products among different observation platforms, both the CALIPSO and PRL profiles are used here. Additionally,~~Thus,~~ a combined profile (gray line) simply ~~assumed to be~~ averaged ~~from~~ between CALIPSO and ~~Lidar~~ PRL~~(gray line)~~ is ~~additionally~~ included. It indicates that aerosols account for about 75% of the totals below 4 km and about 60% in the boundary layer for the combined profile, which to some extent is similar to the default profile of TUV (Palancar and Toselli, 2004). The aerosol DRFs would be~~are all~~ estimated by TUV using all these four profiles.

Figure ~~13~~11

3.4.1 The aerosol direct radiative forcing in ~~both~~ clear ~~and cloudy~~ sky condition~~s~~

DRFs, unless otherwise specified, hereinafter all represent the averaged values among CALIPSO, ~~Lidar~~ PRL and combined profile based forcing in clear sky condition. Figure ~~14~~ 12 shows the seasonal ~~mean~~ variations of the size fractional daytime TOA and surface DRFs of the total, scattering and absorbing aerosols ~~in all, fine and coarse modes in clear sky conditions~~ in urNJNanjing. ~~The scattering aerosol could exert a negative forcing both at TOA and the surface while the absorbing aerosol exerts a positive forcing at TOA and a negative forcing at the surface.~~

~~——~~The aerosol DRFs are highly depended on the aerosol optical properties and compositions. Overall,

the fine aerosols have much more contributions to the total aerosol DRFs, especially for scattering aerosols. The coarse aerosol DRF is only ~15% of the fine aerosol DRF for scattering aerosols while >51% for absorbing aerosols at both the TOA and surface in urNJ. Negative scattering aerosol DRFs could be significantly offset at the TOA while further strengthened at the surface by absorbing aerosols. Therefore, the total coarse aerosol DRF at the TOA is very weak due to a much smaller CSSA and subsequently it has a much smaller contribution to the total aerosol DRF than the fine aerosols. Both the scattering and absorbing aerosol DRFs have similar~~significant~~ seasonality to their AODs~~.~~, peaking in summer for the total scattering aerosols while in spring for the total absorbing aerosols. However, ~~The~~the DRF seasonal variation of each aerosol type is consistent with each other within the same mode, ~~strongest (weakest) forcing at TOA appears~~ all peaking in summer ~~(spring) for~~in fine mode while ~~scattering aerosols and~~ in spring ~~(summer) for~~ in coarse ~~scattering aerosols~~mode. ~~The fine scattering aerosol AOD is about one order of magnitude larger than the coarse one, directly resulting in its much stronger DRFs.~~ In addition to ~~S~~AODs, surface albedo ~~could~~ and the solar zenith angle also have influence on the variation of~~lead to changes in~~ the aerosol DRFs. As implied in Zhuang et al. (2014a), ~~In~~ a brighter surface would yield a weaker negative DRF while a stronger positive DRF~~, the scattering aerosol DRFs might decrease~~ in the condition with fixed ~~loadings or~~ AOD~~s (Zhuang et al., 2014a)~~. The seasonal mean surface albedo averaged from four wavelengths (440, 670, 870 and 1020 nm) ~~are~~ is about 0.145, 0.170, 0.129, and 0.137 in spring, summer, fall, and winter, respectively~~,~~ ~~implying that the scattering aerosol DRFs, to some extent, are weakened in spring and summer due to the higher surface albedo~~. Therefore, ~~The~~ the ~~strongest DRF for the total~~ scattering aerosol~~s~~ DRF is stronger in winter than ~~found in summer, orderly followed by that~~ in ~~winter,~~ spring, although ~~and fall due to the co-affections of SAODs and surface albedo, although~~ SAOD ~~in spring~~ is lower~~higher~~ ~~than~~

772 ~~that~~ in winter. ~~The seasonal variations in the surface scattering aerosol DRFs are consistent with those~~

773 ~~at TOA.~~

774 ~~Similar to the scattering aerosols, the TOA DRFs of the absorbing aerosols are the strongest in summer~~

775 ~~for fine mode and in spring for coarse mode when the aerosol AODs are the highest in the~~

776 ~~corresponding seasons. However, the TOA DRFs are relatively weaker in winter for fine absorbing~~

777 ~~aerosols and in summer and winter for coarse absorbing aerosols.~~ ~~Different from the scattering aerosols,~~

778 ~~the coarse absorbing aerosol DRFs have the same orders of magnitude as the fine ones. DRFs of~~

779 ~~absorbing aerosols are also affected by both the AAODs and surface albedo to a certain degree. Zhuang~~

780 ~~et al. (2014a) stated that higher surface albedo would considerably lead to stronger TOA DRFs and~~

781 ~~weaker surface DRFs for absorbing aerosols with fixed loadings or AAODs, which is different from the~~

782 ~~scattering aerosols. Additionally, the solar zenith angle also plays a considerable role in intensifying~~

783 ~~DRFs. For example, at 8 and 9 pm on 13th Aug in 2011, AAODs and AAEs are all equal to 0.23 and~~

784 ~~1.18, respectively. However, the corresponding DRFs are 3.37 and 4.69 W/m^2 at TOA and 9.12 and~~

785 ~~10.03 W/m^2 at the surface under a condition of the same SSA, surface albedo and aerosol profiles,~~

786 ~~implying that the DRFs would be stronger in warmer seasons or at noon when the optical properties of~~

787 ~~absorbing aerosols and the other affecting factors are fixed.~~ Similarly, ~~Thus,~~ a stronger TOA DRF of

788 the fine absorbing aerosols in spring than in winter might be also related to higher surface albedo and

789 solar zenith angles, although their AAODs in winter are substantially higher. ~~Both fine and coarse~~

790 ~~absorbing aerosol DRFs at TOA are stronger in fall than in winter possibly owing to higher solar zenith~~

791 ~~angles in fall. The all-mode absorbing aerosol DRFs at TOA also have different seasonality from the~~

792 ~~scattering aerosols, being the strongest in spring, orderly followed by those in summer, fall and winter.~~

793 ~~The seasonal variations of the absorbing aerosol DRFs at the surface are somewhat different from at~~

~~TOA in fine and coarse modes.~~ The weakest surface DRF appears in spring for fine absorbing aerosols and in summer for coarse absorbing aerosols possibly due to a higher surface albedo in this season ~~as suggested by Zhuang et al. (2014a)~~. ~~The surface DRFs of the all-mode absorbing aerosols are also the strongest in spring due to the combined effects of the corresponding fine and coarse aerosols.~~

~~The absorbing aerosols can considerably offset the negative DRFs of the scattering aerosols at TOA and strengthen the positive DRFs of the scattering aerosols at the surface (Figures 14a and 14d)~~Unlike the single aerosol type, the total aerosol DRFs are co-affected by both the scattering and absorbing aerosols, meaning that the seasonal variation of the TOA DRF is additionally related to the SSAs' seasonality. Thus, the ~~weakest and~~ strongest TOA DRF~~s~~ of the total fine aerosols appear~~s~~ in ~~spring and~~ winter instead of summer~~, respectively.~~, and t~~T~~he total coarse aerosol DRFs ~~in summer~~ are positive at TOA in summer~~due to a high proportion of absorbing aerosol to the totals (smaller SSA as showed in Figure 3a)~~. For all modes, the seasonal variation of the total aerosol DRFs at TOA are more consistent with that of the fine mode~~, and the DRFs are all weaker than the ones of scattering aerosols~~. Compared with the TOA DRFs of the total aerosols, t~~T~~he variations of surface DRFs ~~of the total fine aerosols~~ are much more consistent with those of corresponding AODs, strongest in summer for fine aerosols while ~~the weakest~~ in spring for coarse aerosols~~, which is opposite to the total coarse aerosols~~. ~~Due to the co-affection of fine and coarse aerosols, t~~The total aerosol DRFs ~~of all-mode aerosols~~ at the surface are the strongest in summer and weakest in fall. ~~The existence of cloud would reduce the solar radiation reaching the surface or lower atmosphere, thus affecting the aerosol DRFs, including their levels and seasonality. This issue would be further addressed in the further.~~

Figure ~~14~~12

To make comparison (Figure 13), ~~Due to lack of the observed SSAs, the absorbing aerosol DRFs here are mainly estimated from the difference between the total and scattering aerosol DRFs. Additionally,~~ absorbing aerosol DRFs based on observed AAOD, AAE and fresh BC SSA (Li et al., 2015b) are also accessed (named as the second way) ~~to investigate the differences between these two types of DRFs as shown in Figure 15~~. Although the absorbing aerosol DRFs are estimated in different ways, they are highly correlated at both the TOA and ~~the~~ surface as shown in the figure~~, implying that they have the same seasonality~~. ~~However~~Apparently, the DRFs from the second method are much weaker than that from the first one~~,~~ possibly due to the absorbing aerosol in urNJ being always in mixed state as analysis in previous section or as indicated in Zhuang et al. (2015). ~~implying that the DRFs from these two methods might represent different mixing states of the absorbing aerosols. Apparently, the second none represents the forcing of fresh absorbing aerosols while the DRFs from the former one might represent the forcing of the aged or internally mixed absorbing aerosols.~~ Jacobson (2000) suggests that the aged (mixed) absorbing aerosols have much stronger ability to absorb solar radiation, with a factor of two. Zhuang et al. (2013a and 2013b) stated that the simulated regional mean TOA DRF~~s~~ of the mixed BC (+1.56 W/m^2) over East Asia is about 1.9 ~~+1.56 W/m^2 for internally mixed BC and about +0.81 W/m^2 for~~times to that of none ~~externally~~ mixed BC. And the ratio is about 1.73 in this study, implying that the absorbing aerosol DRF from the first way is reasonable. Comparison here further proves the importance of the mixing states to estimate the absorbing aerosol ~~direct~~ radiative ~~forcing~~effects.

Figure ~~15~~13

Table 3 lists the annual mean ~~clear sky~~size fractional DRFs of the total, scattering and absorbing aerosols ~~in all, fine and coarse modes~~ at both the TOA and ~~the~~ surface in ~~Nanjing~~urNJ. The DRFs at the surface are all stronger than those at the TOA. The mean DRFs are -10.69, -16.45, 5.76 W/m^2 at TOA and -25.54, -21.37 and -8.38 W/m^2 at the surface for the total, scattering and absorbing aerosols, respectively. The TOA DRFs in fine mode are nearly an order of magnitude stronger than those in coarse mode for the total and scattering aerosols. The DRFs of the fine absorbing aerosols have the same orders of magnitude as, but stronger than those of the coarse absorbing aerosols.

Table 3

~~——~~Various studies on the aerosol DRFs have been carried out based on observations or numerical models. Over all, the DRFs of urban aerosols are much stronger than those on the regional or global scale. Forster et al. (2007) summarized the global mean clear ~~and cloudy~~ sky DRFs of the total aerosols from observations~~, which are~~ being -5.4 ~~and -0.55~~ W/m^2~~, respectively~~. Zhuang et al. (2013a and 2013b) indicated a simulated clear sky DRFs being -4.97 W/m^2 for total aerosols while +1.2 W/m^2 for BC ~~Using a regional climate chemistry model, RegCCMS, Zhuang et al. (2013a and 2013b) estimated the regional mean DRFs of the total and BC aerosols~~ over East Asia ~~and they are -4.97 and +1.2 W/m^2, respectively, in clear sky~~. On a sub-regional or urban scale, observed based analysis showed that the total aerosol DRF always exceeded at least 10^1 W/m^2 (Markowicz et al., ~~(~~2008; Khatri et al., 2009; Wang et al., 2009; Kuhlmann and Quaas, 2010; Alam et al., 2011; Che et al., 2015c, and so on). ~~found that the daytime surface DRF exceeded -20 W/m^2 in Persian Gulf. Khatri et al. (2009) indicated that aerosols exerted a positive DRF of +2.5 W/m^2 at TOA and a strong negative forcing of~~

~~-71.8 W/m^2 at the surface in Nagoya in summer. Alam et al. (2011) found that total aerosol DRFs at TOA was about -22 W/m^2 in Karachi. In East Asia or China, Wang et al. (2009) reported that the TOA DRFs of total aerosols in Beijing are -2, -21 and -16 W/m^2 on clear, haze, and fog days, respectively.~~ Kuhlmann and Quaas (2010) ~~indicated~~ showed that the total aerosol DRFs was about -25 W/m^2 over Qinghai-Tibet Plateau. Che et al. (2014; 2015c) indicated that the daytime total aerosol DRFs in northeast China was about -16.82 W/m^2 while exceeded -30 W/m^2 in both the rural and urban areas of north China Plain in polluted episodes. ~~Che et al. (2014) also reported that the TOA DRFs of the total aerosols in north China Plain exceeded -30 and -40 W/m^2 in rural and urban areas, respectively, during the period with serious haze-fog episodes. Xia et al. (2016) pointed out that the regional mean DRF in China was about -16~-37 W/m^2 at TOA and about -66 ~ -111 W/m^2 at the surface when solar zenith angle was about 60^o. Over all, the DRFs of urban aerosols are much stronger than those on the regional or global scale.~~ Our results show th~~e~~at aerosols in urban area of west YRD could also exert very strong DRF, as large as -25.5 W/m^2 at the surface. Apparently, the DRFs here would have smaller uncertainties than that from simulations because of the use of observations. Compared with the results in Zhuang et al. (2014a), DRFs here might be more precise because: 1. the observed aerosol profiles have not been used; and 2. the absorbed DRFs (might be underestimated) were calculated using fresh BC SSA in Zhuang et al. (2014a)~~same orders of magnitude of DRFs as those for other regions in earlier studies~~. This study further investigates the size fractional (fine and coarse) DRFs of different aerosol components in urban areas of west YRD, which is in favor of better understanding the acts of aerosols affecting solar short wave radiation. And these issues have not been addressed in previous researches. The results here could also be used to validate the numerical simulations to evaluate the model performance on the aerosol radiative effects.

3.4.2 Sensitivity of tThe aerosol direct radiative forcing to varies in different aerosol profiles

Different aerosol profiles might result in different DRFs. Figure 16 14 presents the TOA and surface DRFs of the different aerosol types, including the total, scattering, and absorbing aerosols and the totals, based on four kinds of aerosol profiles from CALIPSO, LidarPRL, Combined CALIPSO and /Lidar PRL shown in Figure 13 11 as well as the default one in TUV (Palancar and Toselli, 2004) in clear sky condition. The figure shows that the aerosol direct raidative forcingDRFs in clear sky condition is not very sensitive to the aerosol profiles, although the differences among absorbing aerosol TOA-DRFs , are more sensitive than scattering aerosolsfrom different profiles are more obvious to some degree than the scattering aerosol DRFs or the surface forcing. Overall, both the scattering and absorbing aerosol DRFs at TOA would become weaker to some extent if more aerosols were concentrated in lower layers of atmosphere or within boundary layer especially for the latter one. Here, a profile impact factor: PIF is defined as the ratio of the standard deviations among the four types of DRFs in Figure 16 14 to the averaged values among these four DRFs. The PIF is about 4.97% for absorbing aerosol TOA-DRF while below 2% for the rest types of DRFs during the study period, further proving the weak influence of the aerosol profile on the clear sky DRFs. Overall, both the scattering and absorbing aerosol DRFs at TOA would become weaker to some extent if more aerosols were concentrated in lower layers of atmosphere or within boundary layer especially for the absorptions, implying that the aerosol profiles might also become significant in some extreme cases (high level of aerosol appearing very low layers in serious pollution episodes). In contrast, tThe aerosol profiles might have much more influence on the DRFs in cloudy sky condition because the absorbing aerosols over brighter cloud would absorb more short wave radiation (Podgorny and Ramanathan,

2001). This issue is also going to be addressed in the further.

Figure ~~16~~14

3.4.3 Briefly discussions

Although the observation based DRFs of the total, scattering and absorbing aerosols, as well as their sensitivities to the aerosol profiles are analyzed in this study~~,~~; uncertainties still exist due to the measurement errors of the optical properties mentioned in Section 2. Additional estimations of the aerosol DRFs are carried out based on the errors of AOD, AAOD and SSAs. Results indicate that larger uncertainties of the aerosol DRFs are mainly derived from the errors of SSA or AAOD. Uncertainty of total aerosol AOD (0.01) only yield about 1% relative bias for the total aerosol DRFs at both the TOA and surface. The total or fine aerosol SSA error (0.03 or 0.037) may result in about 24% uncertainties at the TOA (<15% at the surface) to the corresponding DRFs. A larger coarse aerosol SSA error (0.085) leads to a ~24% uncertainties of its surface DRFs. AAOD errors (0.01) cause about 20% uncertainties to the absorbing DRFs at both the TOA and surface, while only 1.2% to the scattering DRFs. Overall, these uncertainties are relatively smaller than those presented in 5th IPCC report (IPCC, 2013) and they could be further decreased if the measurements or the algorithms were further improved. In addition to the uncertainties, this study ~~there~~ still exist limitations to be addressed in the future. First, the absorbing aerosol SSA should be further measured to better estimate corresponding DRFs ~~are estimated from the difference between the total and scattering aerosol DRFs. The methods are still with uncertainties to some extent. Therefore, the observed SSA of the absorbing aerosols is needed in further studies to enhance the accuracy.~~ Second, the DRF would be a little more precise ~~uncertainty can be~~

~~further reduced~~ if ~~data with~~ the aerosols profiles with higher temporal resolutions ~~of the aerosols profiles are~~ were used instead of ~~to substitute~~ their annual means. Third, long-term trends of the aerosol optical properties and direct radiative forcing, including their interannual and interdecadal variations, should be taken into consideration. Finally, extremely high aerosol loadings are frequently observed in serious pollution episodes, including dust storms, biomass burning, and regional transport (Zhuang et al., 2014a, b and 2015). The aerosol optical and physical properties as well as the radiative forcing would be rather different in these extreme episodes, which also deserve further studies.

4 Conclusions

In this study, the size fractional aerosol optical and physical properties observed by Cimel sun photometer (CE-318), as well as ~~its~~ corresponding direct radiative forcing (DRF) calculated by a radiation transfer model TUV based on observations~~ed aerosol optical properties, profiles, and surface albedo~~ in urban area of Nanjing (urNJ), west YRD, are investigated.

In urban area of west YRD, t~~T~~he annual mean total aerosol ~~optical depths~~AOD at 550 nm ~~,~~ ~~is~~are 0.65, mostly contributed by the scattering components (0.61). The absorption fraction is as small as about ~6.7%, changing with the seasons~~, and 0.04 for the total (AOD), scattering (SAOD) and absorbing (AAOD) aerosols, respectively~~. There are about 80% of aerosols distributing in fine mode in urNJ during the sampling periods. The absorption fraction is about 4.6% in fine mode while 15.5% in coarse mode, showing a very different compositions and absorption characteristics of these two kinds of aerosols. ~~The fine mode fractions of the total, scattering and absorbing aerosols are 81.53%, 81.97% and 56.09%, respectively. The absorbing aerosols are finer, with an Ångström exponent (AE) of 1.32 at 440/870 nm, 0.13 (0.12) larger than the scattering (total) aerosols. Fine aerosol AEs are much larger~~

948 ~~than coarse one, especially for scattering aerosols. Additionally, the fine aerosol is more scattering~~

949 ~~(SSA=0.95) while the coarse aerosol more absorption (SSA=0.82). The mean 440 nm refractive index~~

950 ~~is about 1.44+0.0084i during the study period.~~ Compared with the satellite retrievals, the aerosol

951 optical properties here have much higher temporal resolutions and products~~AOD and AE observed by~~

952 ~~CE 318 are rather similar to those from MODIS. AAOD and AAE from CE 318 to some extent are~~

953 ~~related to the surface aerosol absorption coefficient (AAC) and AAE. The aerosols in Nanjing have~~

954 ~~smaller AOD than, but the same AE as, and are more scattering than, those in coastal cities of YRD~~.

955 Further analysis on the aerosol optical properties indicates that there might be about 15% and 27%

956 occurrence of dust dominated and BC dominated mixing aerosols, respectively, in west YRD during the

957 observed period.

958 ~~The aerosol optical properties have significant seasonality. AOD and AE of scattering aerosols are~~

959 ~~lowest in fall and in spring while highest in summer and fall, respectively. The highest AAOD and~~

960 ~~AAE appear in spring and winter while the lowest ones are found in fall and summer. Fine mode AOD~~

961 ~~are all at maximum in summer but minimum in spring, while coarse AOD are at maximum in spring.~~

962 ~~The AEs in both fine and coarse modes are closer to zero in summer than those in the other seasons due~~

963 ~~to the effects of high humidity. The total aerosol AOD and AE seasonality is consistent with the~~

964 ~~scattering aerosols. However, the smallest SSA is found in spring, although both FSSA and CSSA are~~

965 ~~relative smaller in summer. All AODs and SSAs follow a near lognormal pattern and almost all of the~~

966 ~~AE and refractive indices follow a unimodal pattern. The ranges around their means dominated,~~

967 ~~accounting for at least 60% to their total data samples during the entire study period. They also have~~

968 ~~substantial seasonality.~~

969 ~~——~~The aerosols in west YRD~~Nanjing~~ have a two-mode lognormal pattern in volume size

970 distribution~~, with substantial seasonality,~~ peaking at the radius of 0.148 and 2.94 μm in annual scale.
971 Both the fine and coarse particles have the same contribution to the totals at lower aerosol loadings
972 (AOD<0.8). In higher AOD (>0.8) levels, the fine aerosols are predominate. Results further indicate
973 that the fine or coarse aerosol could individually induce a very serious polluted episode in urban region
974 of west YRD. ~~The fine (coarse) mode peak has a leftward (rightward) shift relative to the annual peaks~~
975 ~~in spring while both of them have a right ward shift in summer. AOD show a positive dependence on~~
976 ~~the volume concentrations in both fine and coarse modes. The peaks would be close to each other with~~
977 ~~increasing AOD.~~ Both the fine and coarse aerosols have the same level of volume concentrations,
978 although their ~~mean effective~~ radiuses differ by an order of magnitude~~of fine aerosol is an order of~~
979 ~~magnitude smaller than the coarse one~~. ~~The mean effective radius and volume concentrations of the all~~
980 ~~modes are 0.34μm and 0.24 $\mu m^3/cm^3$, respectively, all peaking in spring. It's well known that the~~
981 ~~seasonality of the radius are anti-correlated well with the AEs.~~

982 The mean DRF~~s~~ of the total aerosols ~~are~~ is -10.69~~, -16.45, -5.76~~ W/m^2 at the TOA and -25.54~~,~~
983 ~~-21.37 and -8.38~~ W/m^2 at the surface ~~for the total, scattering and absorbing aerosols, respectively~~, in
984 clear sky condition. The fine ~~mode~~ aerosol DRF~~s~~ ~~at TOA~~ accounts for more than 97% of the totals at
985 the TOA~~are nearly an order of magnitude larger than the coarse ones for scattering aerosols while they~~
986 ~~have the same levels for absorbing aerosols~~. Estimations on the size fractional DRF of each aerosol
987 component indicate that the coarse aerosol DRF is only ~15% of the fine one within scattering aerosols
988 while >51% within absorbing aerosols at both the TOA and surface in urNJ. The DRFs estimated for
989 ~~urban Nanjing~~urNJ in this study are much stronger than ~~those on~~ their regional or global ~~scales~~means.

990 ~~——~~The size fractional aerosol optical, physical properties and DRFs have significant seasonality
991 in west YRD. The DRF variations of each aerosol type within the same mode are mostly consistent

with the variations of corresponding AODs, all peaking in summer for the fine aerosols while in spring for the coarse ones. However, the variations of total aerosol DRF at the TOA are different from corresponding AOD within the same size segment because negative DRFs of the scattering are always offset by absorbing aerosol. Both the fine and coarse aerosols have the largest size and are the most absorbing in summer, which are different from the whole mode aerosols (in spring). ~~The seasonal variations of the DRFs, to some extent, are different between at TOA and the surface, between the scattering and absorbing aerosols, as well as between the fine and coarse modes. In clear sky condition, both the TOA and surface DRFs of scattering and absorbing aerosols are all the strongest in summer for fine mode and in spring for coarse one. However, the largest DRF value appears in spring for total scattering aerosols whereas in spring for total absorbing aerosols due to different fine mode fractions of these two types of aerosols in different seasons, which further results in the strongest (weakest) DRFs of all aerosols found in winter (spring) at the TOA and in summer (fall) at the surface due to different fractions of scattering aerosols to the total aerosols.~~

The ~~sensitivity~~ sensitivities of clear sky aerosol DRFs ~~on~~ to the aerosol profiles ~~is~~ are not significant ~~in clear sky condition,~~ ~~and the bias is~~ all smaller than~~about~~ 5% ~~for the TOA DRFs of absorbing aerosol while less 2% for the rest DRFs~~. Overall, both scattering and absorbing aerosol DRFs at TOA would become a little weaker to some extent if more aerosols were concentrated in lower layers of atmosphere ~~or within boundary layer~~, especially for the absorbed DRF~~ption~~. Further investigation suggests that another uncertainty of the DRFs is from the measuring errors of the aerosol optical properties. Larger biases are mainly from the errors of SSA and AAOD.

Acknowledgements: This work was supported by the National Key Basic Research Development

Program of China (2017YFC0209803, 2014CB441203, 2016YFC0203303), the National Natural Science Foundation of China (41675143, 91544230, 41621005), the New Teachers' Fund for Postdoctoral Fellows, Ministry of Education (20120091120031), FP7 project: REQUA (PIRSES-GA-2013-612671), and a project Funded by the Priority Academic Program Development of the Jiangsu Higher Education Institutions (PAPD). The authors would like to thank all members in the AERC of Nanjing University for maintaining instruments.

5 References

Alam, K., Trautmann, T., and Blaschke, T.: Aerosol optical properties and radiative forcing over mega-city Karachi. Atmos. Res. 101, 773-782, 2011.

Angström, A.: On the atmospheric transmission of sun radiation and on dust in the air, Geogr. Ann., 11, 156–166, 1929.

Arnott, W. P., Hamasha, K., Moosmuller, H., Sheridan, P. J., and Ogren, J. A.: Towards aerosol light-absorption measurements with a 7-wavelength aethalometer: evaluation with a photoacoustic instrument and 3-wavelength nephelometer, Aerosol Sci. Tech., 39, 17–29, doi:10.1080/027868290901972, 2005.

Bellouin, N., Boucher, O., Tanré, D., and Dubovik, O.: Aerosol absorption over the clear-sky oceans deduced from POLDER-1 and AERONET observations, Geophys. Res. Lett., 30, 1748, doi:10.1029/2003GL017121, 2003.

Bergin, M. H., Cass, G. R., Xu, J., Fang, C., Zeng, L., Yu, T., Salmon, L. G., Kiang, C. S., Tang, X. Y., Zhang, Y. H., and Chameides, W. L.: Aerosol radiative, physical, and chemical properties in Beijing during June 1999, J. Geophys. Res., 106 (D16), 17969–17980, 2001.

1036 Cai, H. K., Zhou, R. J., Fu, Y. F., Zheng, Y. Y., and Wang, Y. J.: Cloud-aerosol lidar with or thogonal
1037 polarization detection of aerosol optical properties after a crop burning case, Clim. Environ. Res.,
1038 16, 469–478, 2011.
1039 Che, H. Z., Zhang, X. Y., Xia, X., Goloub, P., Holben, B., Zhao, H., Wang, Y., Zhang, X. C., Wang, H.,
1040 Blarel, L., Damiri, B., Zhang, R., Deng, X., Ma, Y., Wang, T., Geng, F., Qi, B., Zhu, J., Yu, J., Chen,
1041 Q., and Shi, G.: Ground-based aerosol climatology of China: aerosol optical depths from the China
1042 Aerosol Remote Sensing Network (CARSNET) 2002–2013, Atmos. Chem. Phys., 15, 7619–7652,
1043 2015a.
1044 Che, H. Z., Zhao, H. J., Wu, Y. F., Xia, X. A., Zhu, J., Wang, H., Wang, Y. Q., Sun, J. Y., Yu, J., Zhang,
1045 X. Y., and Shi, G. Y.: Analyses of aerosol optical properties and direct radiative forcing over urban
1046 and industrial regions in Northeast China, Meteorology and Atmospheric Physics, 127(3), 345-354,
1047 doi:10.1007/s00703-015-0367-3, 2015c.
1048 Che, H., Wang, Y., and Sun, J.: Aerosol optical properties at Mt. Waliguan observatory, China, Atmos.
1049 Environ., 45, 6004–6009, 2011.
1050 Che, H., Xia, X., Zhu, J., Li, Z., Dubovik, O., Holben, B., Goloub, P., Chen, H., Estelles, V.,
1051 Cuevas-Agulló, E., Blarel, L., Wang, H., Zhao, H., Zhang, X., Wang, Y., Sun, J., Tao, R., Zhang, X.,
1052 and Shi, G.: Column aerosol optical properties and aerosol radiative forcing during a serious
1053 haze-fog month over North China Plain in 2013 based on ground-based sunphotometer
1054 measurements, Atmos. Chem. Phys., 14, 2125–2138, doi:10.5194/acp-14-2125-2014, 2014.
1055 Che, H., Xia, X., Zhu, J., Wang, H., Wang, Y., Sun, J., Zhang, X., and Shi, G.: Aerosol optical
1056 properties under the condition of heavy haze over an urban site of Beijing, China, Environ. Sci.
1057 Pollut. R., 22, 1043–1053, doi:10.1007/s11356-014-3415-5, 2015b.

Che, H.,Wang, Y., Sun, J., Zhang, X., Zhang, X., and Guo, J.: Variation of Aerosol Optical Properties over the Taklimakan Desert in China, Aerosol Air Qual. Res., 13, 777–785, 2013.

Chiang, C. W., Chen, W. N., Liang, W. A., Das, S. K., and Nee, J. B.: Optical properties of tropospheric aerosols based on measurements of lidar, sun-photometer, and visibility at Chung-Li (25°N, 121°E), Atmos. Environ., 41, 4128-4137, doi:10.1016/j.atmosenv.2007.01.019, 2007.

Deng, J. J., Zhang, Y. R., Hong, Y. W., Xu, L. L., Chen, Y. T., Du, W. J., and Chen, J. S.: Optical properties of $PM_{2.5}$ and the impacts of chemical compositions in the coastal city Xiamen in China, Science of the Total Environment, 557-558, 665-675, 2016.

Dubovik, O. and King, M. D.: A flexible inversion algorithm for the retrieval of aerosol optical properties from Sun and sky radiance measurements, J. Geophys. Res., 105, 20673–20696, doi:10.1029/2000JD900282, 2000.

Dubovik, O., Sinyuk, A., Lapyonok, T., Holben, B. N., Mishchenko, M., Yang, P., Eck, T. F., Volten, H., Munoz, O., Veihelmann, B., van der Zande, W. J., Leon, J. F., Sorokin, M., and Slutsker, I.: Application of spheroid models to account for aerosol particle nonsphericity in remote sensing of desert dust, J. Geophys. Res.-Atmos., 111, D11208, doi:10.1029/2005jd006619, 2006.

Fan, X. H., Chen, H. B., Xia, X. A., Li, Z. Q., and Cribb, M.: Aerosol optical properties from the Atmospheric Radiation Measurement Mobile Facility at Shouxian. China, J. Geophys. Res., 115, D00K33, doi:10.1029/2010JD014650, 2010.

Forster, P., Ramaswamy, V., Artaxo, P., Berntsen, T., Betts, R., Fahey, D. W., Haywood, J., Lean, J., Lowe, D. C., Myhre, G., Nganga, J., Prinn, R., Raga, G., Schulz, M., and Van Dorland, R.: Changes in atmospheric constituents and in radiative forcing, in: Climate Change 2007: The Physical Science Basis. Contribution of Working Group I to the Fourth Assessment Report of the

Intergovernmental Panel on Climate Change, edited by: Solomon, S. et al., Cambridge Univ. Press, Cambridge, UK, 129–234, 2007.

Hansen, A. D. A., Rosen, H., and Novakov, T.: The aethalometer: an instrument for the real time measurements of optical absorption by aerosol particles, Sci. Total Environ., 36, 191–196, 1984.

He, X., Li, C. C., Lau, A. K. H., Deng, Z. Z., Mao, J. T., Wang, M. H., and Liu, X. Y.: An intensive study of aerosol optical properties in Beijing urban area, Atmos. Chem. Phys., 9, 8903–8915, doi:10.5194/acp-9-8903-2009, 2009.

Holben, B. N., Eck, T. F., Slutsker, I., Tanre, D., Buis, J. P., Setzer, A., Vermote, E., Reagan, J. A., Kaufman, Y. J., Nakajima, T., Lavenu, F., Jankowiak, I., and Smirnov, A.: AERONET-a federated instrument network and data archive for aerosol characterization, Remote Sens. Environ., 66, 1-16, 1998.

Holler, R., Ito, K., Tohno, S., and Kasahara, M.: Wavelength-dependent aerosol single scattering albedo: measurements and model calculations for a coastal site near the sea of Japan during ACE-Asia, J. Geophys. Res., 108, 8648, doi:10.1029/2002JD003250, 2003.

IPCC 2013: Climate Change 2013: The Physical Science Basis. Contribution of Working Group I to the Fifth Assessment Report of the Intergovernmental Panel on Climate Change, edited by: Stocker, T. F., Qin, D., Plattner, G.-K., Tignor, M., Allen, S. K., Boschung, J., Nauels, A., Xia, Y., Bex, V., and Midgley, P. M., Cambridge University Press, Cambridge, UK and New York, NY, USA, 1535 pp., 2013.

Jacobson, M. Z.: A physically based treatment of elemental carbon optics: implication for global direct forcing of aerosols, Geophys. Res. Lett., 27, 217-220, 2000.

Jacobson, M. Z.: Control of fossil-fuel particulate black carbon and organic matter, possibly the most

effective method of slowing global warming, J. Geophys. Res., 107, 4410, doi:10.1029/2001JD001376, 2002.

Jiang, Z., Liu, Z., Wang, T., Schwartz, C. S., Lin, H.-C., and Jiang, F.: Probing into the impact of 3DVAR assimilation of surface PM_{10} observations over China using process analysis, J. Geophys. Res. Atmos., 118, 6738–6749, doi:10.1002/jgrd.50495, 2013.

Khatri, P., Ishizaka, Y., and Takamura, T.: A study on aerosol optical properties in an urban atmosphere of Nagoya, Japan. J. Meteorol. Soc. Jpn., 87 (1), 19-38, 2009.

Kiehl, J. T. and Briegleb, B. P.: The relative roles of sulfate aerosols and greenhouse gases in climate forcing, Science, 260, 311–314, 1993.

Kuhlmann, J., and Quaas, J.: How can aerosols affect the Asian summer monsoon? Assessment during three consecutive pre-monsoon seasons from CALIPSO satellite data, Atmos. Chem. Phys., 10, 4673-4688, doi:10.5194/acp-10-4673-2010, 2010.

Li, J., Carlson, B. E., and Lacis, A. A.: Using single-scattering albedo spectral curvature to characterize East Asian aerosol mixtures, J. Geophys. Res. Atmos., 120, 2037–2052, 2015c.

Li, J., Wang, W.-C., Liao, H., and Chang, W. Y.: Past and future direct radiative forcing of nitrate aerosol in East Asia, Theor. Appl. Climatol., 121, 445–458, 2015b.

Li, S., Wang, T. J., Xie, M., Han, Y., and Zhuang, B. L.: Observed aerosol optical depth and angstrom exponent in urban area of Nanjing, China, Atmos. Environ., 123, 350-356, doi:10.1016/j.atmosenv.2015.02.048, 2015a.

Liao, H. and Seinfeld, J. H.: Global impacts of gas-phase chemistry-aerosol interactions on direct radiative forcing by anthropogenic aerosols and ozone, J. Geophys. Res., 110, D18208, doi:10.1029/2005JD005907, 2005.

1124 Ma, X. X., Liu, H. N., Liu, J., and Zhuang, B. L.: Sensitivity of climate effects of black carbon in China
1125 to its size distributions, Atmospheric Research, 185, 118-130, 2017.
1126 Ma, X., and Yu, F.: Effect of spectral dependent surface albedo on Saharan dust direct radiative forcing.
1127 Geophys. Res. Lett. 39, L09808, 2012.
1128 Madronich, S.: UV radiation in the natural and perturbed atmosphere, In: Tevini,M. (Ed.), UV-B
1129 Radiation and Ozone Depletion, Effects on Humans, Animals, Plants, Microorganisms, and
1130 Materials, Lewis Publisher, Boca Raton, pp. 17-69, 1993.
1131 Markowicz, K. M., Flatau, P. J., Remiszewska, J., Witek, M., Reid, E. A., Reid, J. S., Bucholtz, Z., and
1132 Hilben, B.: Observations and modeling of the surface aerosol radiative forcing during UAE. J.
1133 Atmos. Sci. 65, 2877-2891, 2008.
1134 Menon, S., Hansen, J., Nazarenko, L., and Luo, Y. F.: Climate effects of black carbon aerosols in China
1135 and India, Science, 297, 2250–2253, doi:10.1126/science.1075159, 2002.
1136 Palancar, G.G., and Toselli, B. M.: Effects of meteorology and tropospheric aerosols on UV-B radiation:
1137 a 4-year study. Atmos. Environ. 18, 2749-2757, 2004.
1138 Pan, L, Che, H. Z., Geng, F. H., Xia, X. A., Wang, Y. Q., Zhu, C. Z., Chen, M., Gao, W., and Guo, J. P.:
1139 Aerosol optical properties based on ground measurements over the Chinese Yangtze Delta Region,
1140 Atmos. Environ., 44, 2587-2596, doi:10.1016/j.atmosenv.2010.04.013, 2010.
1141 Peng, Z., Liu, Z. Q., Chen, D., and Ban, J. M: Improving PM2:5 forecast over China by the joint
1142 adjustment of initial conditions and source emissions with an ensemble Kalman filter, Atmos. Chem.
1143 Phys., 17, 4837–4855, 2017.
1144 Penner, J. E., Andreae, M., Annegarn, H., Barrie, L., Feichter, J., Hegg, D., Jayaraman, A., Leaitch, R.,
1145 Murphy, D., Nganga, J., and Pitari, G.: Aerosols, their direct and indirect effects, in: Climate

1146 Change 2001: The Scientific Basis. Contribution of Working Group I to the Third Assessment
1147 Report of the Intergovernmental Panel on Climate Change, edited by: Houghton, J. T. et al.,
1148 Cambridge University Press, Cambridge, UK and New York, NY, USA, 289–348, 2001.
1149 Podgorny, I. A., and Ramanathan, V.: A modeling study of the direct effect of aerosols over the
1150 tropical Indian Ocean, J Geophys. Res. 106, D20, 24097–24105, 2001.
1151 Qi, B., Hu, D. Y., Che, H. Z., Du, R. G., Wu, Y. F., Xia, X. A., Zha, B., Liu, J., Niu, Y. W., Wang, H.,
1152 Zhang, X. Y., and Shi, G. Y.: Seasonal variation of aerosol optical properties in an urban site of the
1153 Yangtze Delta Region of China. Aerosol Air Qual. Res., 16, 2884-2896, 2016.
1154 Reddy, M. S., Boucher, O., Bellouin, N., Schulz, M., Balkanski, Y., Dufresne, J. L., and Pham, M.:
1155 Estimates of global multicomponent aerosol optical depth and direct radiative perturbation in the
1156 Laboratoire de Meteorologie Dynamique general circulation model, J. Geophys. Res., 110, D10S16,
1157 doi:10.1029/2004JD004757, 2005.
1158 Russell, P. B., Kacenelenbogen, M., Livingston, J. M., Hasekamp, O. P., Burton, S. P., Schuster, G. L.,
1159 Johnson, M. S., Knobelspiesse, K. D., Redemann, J., Ramachandran, S., and Holben, B.: A
1160 multiparameter aerosol classification method and its application to retrievals from spaceborne
1161 polarimetry, J. Geophys. Res.-Atmos., 119, 9838–9863, doi:10.1002/2013JD021411, 2014.
1162 Sun, H., Pan, Z., and Liu, X.: Numerical simulation of spatial-temporal distribution of dust aerosol and
1163 its direct radiative effects on East Asian climate, J. Geophys. Res., 117, D13206,
1164 doi:10.1029/2011JD017219, 2012.
1165 Tao, R., Che, H. Z., Chen, Q. L., Tao, J., Wang, Y. Q., Sun, J. Y., Wang, H., and Zhang, X. X.: Study of
1166 aerosol optical properties based on ground measurements over Sichuan Basin, China, Aerosol and
1167 Air Quality Research, 14: 905–915. doi:10.4209/aaqr.2012.07.0200, 2014.

1168 Wang, T. J., Zhuang, B. L., Li, S., Liu, J., Xie, M., Yin, C. Q., Zhang, Y., Yuan, C., Zhu, J. L., Ji, L. Q.,
1169 and Han, Y.: The interactions between anthropogenic aerosols and the East Asian summer monsoon
1170 using RegCCMS, J. Geophys. Res. Atmos., 120, doi:10.1002/2014JD022877, 2015.
1171 Wang, Y., Che, H. Z., Ma, J. Z., Wang, Q., Shi, G. Y., Chen, H. B., Goloub, P., and Hao, X. J.: Aerosol
1172 radiative forcing under clear, hazy, foggy, and dusty weather conditions over Beijing, China,
1173 Geophys. Res. Lett., 36, L06804, doi:10.1029/2009GL037181, 2009.
1174 Weingartner, E., Saathoff, H., Schnaiter, M., Streit, N., Bitnar, B., and Baltensperger, U.: Absorption of
1175 light by soot particles: determination of the absorption coefficient by means of aethalometers, J.
1176 Aerosol Sci., 34, 1445–1463, doi:10.1016/S0021-8502(03)00359-8, 2003.
1177 Wu, Y. F., Zhang, R. J., Pu, Y. F., Zhang, L. M., Ho, K. F., and Fu, C. B.: Aerosol optical properties
1178 observed at a semi-arid rural site in northeastern China, Aerosol Air Qual. Res., 12, 503–514, 2012.
1179 Xia, X. A., Li, Z. Q., Holben, B., Wang, P., Eck, T., Chen, H. B., Cribb, M., and Zhao, Y. X.: Aerosol
1180 optical properties and radiative effects in the Yangtze Delta region of China, J. Geophys. Res., 112,
1181 D22S12, doi:10.1029/2007JD008859, 2007.
1182 Xia, X., Che, H., Zhu, J., Chen, H., Cong, Z., Deng, X., Fan, X., Fu, Y., Goloub, P., Jiang, H., Liu, Q.,
1183 Mai, B., Wang, P., Wu, Y., Zhang, J., Zhang, R., and Zhang, X.: Ground-based remote sensing of
1184 aerosol climatology in China: aerosol optical properties, direct radiative effect and is
1185 parameterization, Atmos. Environ., 214, 243-251, doi:10.1016/j.atmosenv.2015.06.071, 2016.
1186 Xu, J., Bergin, M. H., Greenwald, R., Schauer, J. J., Shafer, M. M., Jaffrezo, J. L., and Aymoz, G.:
1187 Aerosol chemical, physical, and radiative characteristics near a desert source region of Northwest
1188 China during ACE-Asia, J. Geophys. Res., 109, D19S03, doi:10.1029/2003JD004239, 2004.
1189 Xu, J., Bergin, M. H., Yu, X., Liu, G., Zhao, J., Carrico, C. M., and Baumann, K.: Measurement of

aerosol chemical, physical and radiative properties in the Yangtze delta region of China, Atmos. Environ., 36, 161–173, 2002.

Xu, J., Tao, J., Zhang, R., Cheng, T., Leng, C., Chen, J., Huang, G., Li, X., and Zhu, Z.: Measurements of surface aerosol optical properties in winter of Shanghai, Atmos. Res., 109-110, 25–35, 2012.

Xu, X.: Retrieval of aerosol microphysical properties from AERONET photolarimetric measurements. PhD diss., Department of Earth and Atmospheric Sciences, University of Nebraska-Lincoln, 2015.

Yan, P., Tang, J., Huang, J., Mao, J. T., Zhou, X.J., Liu, Q., Wang, Z. F., and Zhou, H. G.: The measurement of aerosol optical properties at a rural site in Northern China, Atmos. Chem. Phys., 8, 2229–2242, doi:10.5194/acp-8-2229-2008, 2008.

Yu, J., Che, H. Z., Chen, Q. L., Xia, X. A., Zhao, H. J., Wang, H., Wang, Y. Q., Zhang, X. X., and Shi, G. Y.: Investigation of aerosol optical depth (AOD) and Ångström exponent over the desert region of northwestern China based on measurements from the China Aerosol Remote Sensing Network (CARSNET), Aerosol Air Qual. Res., 15, 2024-2036, doi:10.4209/aaqr.2014.12.0326, 2015.

Yu, X. N., Ma, J., Kumar, K. R., Zhu, B., An, J. L., He, J. Q., and Li, M.: Measurement and analysis of surface aerosol optical properties over urban Nanjing in the Chinese Yangtze River Delta, Sci. Total Environ., 542, 277-291, 2016.

Yu, X. N., Zhu, B., Yin, Y., Fan, S. X., and Chen, A. J.: Seasonal variation of columnar aerosol optical properties in Yangtze River Delta in China, Adv. Atmos. Sci., 28(6), 1326-1335, doi:10.1007/s00376-011-0158-9, 2011.

Zhang, L., Sun, J. Y., Shen, X. J., Zhang, Y. M., Che, H., Ma, L. Q., Zhang, Y. W., Zhang, X. Y., and Ogren, J. A.: Observations of relative humidity effects on aerosol light scattering in the Yangtze River Delta of China, Atmos. Chem. Phys., 15, 8439–8454, 2015.

1212 Zhang, Q., Streets, D. G., Carmichael, G. R., He, K. B., Huo, H., Kannari, A., Klimont, Z., Park, I. S.,
1213 Reddy, S., Fu, J. S., Chen, D., Duan, L., Lei, Y., Wang, L. T., and Yao, Z. L.: Asian emissions in
1214 2006 for the NASA INTEX-B mission, Atmos. Chem. Phys., 9, 5131–5153,
1215 doi:10.5194/acp-9-5131-2009, 2009.
1216 Zhang, W., Hu, B., Chen, C. H., Du, P., Zhang, L., and Feng, G. H.: Scattering properties of
1217 atmospheric aerosols over Lanzhou City and applications using an integrating nephelometer, Adv.
1218 Atmos. Sci., 21(6), 848–856, 2004.
1219 Zhang, X. Y., Wang, Y. Q., Niu, T., Zhang, X. C., Gong, S. L., Zhang, Y. M., and Sun, J. Y.:
1220 Atmospheric aerosol compositions in China: Spatial/temporal variability, chemical signature,
1221 regional haze distribution and comparisons with global aerosols, Atmos. Chem. Phys., 12, 779–799,
1222 doi:10.5194/acp-12-779-2012, 2012.
1223 Zhao, H. J., Che, H. Z., Zhang, X. Y., Ma, Y. J., Wang, Y. F., Wang, X. X., Liu, C., Hou, B., and Che,
1224 X. C.: Aerosol optical properties over urban and industrial region of Northeast China by using
1225 ground-based sun-photometer Measurement, Atmos. Environ., 75, 270-278.
1226 doi:10.1016/j.atmosenv.2013.04.048, 2013.
1227 Zheng, Y., Che, H. Z., Zhao, T. L., Xia, X. A., Gui, K., An, L. C., Qi, B., Wang, H., Wang, Y. Q., Yu, J.,
1228 and Zhang, X. Y.: Aerosol optical properties during the World Athletics Championships and Victory
1229 Day Military Parade over Beijing in August and September 2015, Atmosphere, 7(3), 47;
1230 doi:10.3390/ atmos7030047, 2016.
1231 Zhu, J., Che, H. Z., Xia, X. A., Chen, H. B., Goloub, P., and Zhang, W. X.: Column-integrated aerosol
1232 optical and physical properties at a regional background atmosphere in North China Plain, Atmos.
1233 Environ., 84, 54-64, doi:10.1016/j.atmosenv.2013.11.019, 2014.

1234 Zhu, J., Wang, T., Talbot, R., Mao, H., Hall, C. B., Yang, X., Fu, C., Zhuang, B., Li, S., Han, Y., and
1235 Huang, X.: Characteristics of atmospheric Total Gaseous Mercury (TGM) observed in urban
1236 Nanjing, China, Atmos. Chem. Phys., 12, 12103–12118, doi:10.5194/acp-12-12103-2012, 2012.
1237 Zhuang, B. L., Li, S., Wang, T. J., Deng, J. J., Xie, M., Yin, C. Q., and Zhu, J. L.: Direct radiative
1238 forcing and climate effects of anthropogenic aerosols with different mixing states over China,
1239 Atmos. Environ., 79, 349–361, doi:10.1016/j.atmosenv.2013.07.004, 2013a.
1240 Zhuang, B. L., Liu, Q., Wang, T. J., Yin, C. Q., Li, S., Xie, M., Jiang, F., and Mao, H. T.: Investigation
1241 on semi-direct and indirect climate effects of fossil fuel black carbon aerosol over China, Theor.
1242 Appl. Climatol., 114, 651–672, doi:10.1007/s00704-013-0862-8, 2013b.
1243 Zhuang, B. L., Wang, T. J., Li, S., Liu, J., Talbot, R., Mao, H. T., Yang, X. Q., Fu, C. B., Yin, C. Q.,
1244 Zhu, J. L., Che, H. Z., and Zhang, X. Y.: Optical properties and radiative forcing of urban aerosols
1245 in Nanjing, China, Atmos. Environ., 83, 43–52, 2014a.
1246 Zhuang, B. L., Wang, T. J., Liu, J., Li, S., Xie, M., Han, Y., Chen, P. L., Hu, Q. D., Yang, X. Q., Fu, C.
1247 B., Zhu, J. L.: The surface aerosol optical properties in urban area of Nanjing, west Yangtze River
1248 Delta, China, Atmos. Chem. Phys., 17, 1143–1160, 2017.
1249 Zhuang, B. L., Wang, T. J., Liu, J., Li, S., Xie, M., Yang, X. Q., Fu, C. B., Sun, J. N., Yin, C. Q., Liao, J.
1250 B., Zhu, J. L., and Zhang, Y.: Continuous measurement of black carbon aerosol in urban Nanjing of
1251 Yangtze River Delta, China, Atmos. Environ., 89, 415–424, 2014b.
1252 Zhuang, B. L., Wang, T. J., Liu, J., Ma, Y., Yin, C. Q., Li, S., Xie, M., Han, Y., Zhu, J. L., Yang, X. Q.,
1253 and Fu, C. B.: Absorption coefficient of urban aerosol in Nanjing, west Yangtze River Delta, China,
1254 Atmos. Chem. Phys., 15, 13633–13646, 2015.
1255

Figure captions:

Figure 1. Monthly variations of the total (a), scattering (b), and absorbing (c) aerosol optical depths (AOD) at 550 nm, including the ratio of the AOD in fine or coarse mode to the AOD in all mode (line with triangle markers in green) in urban area of Nanjing. The 10th, 25th, median, 75th, 90th percentile values of the all mode AOD are presented as box plots. The monthly means of the all mode AODs are presented as cycle markers in gray.

Figure 2. Monthly variations of the total (a), scattering (b), and absorbing aerosol (c) Ångström exponents (AE) at 440/870 nm for the all, fine and coarse modes in urban area of Nanjing.

Figure 3. Monthly variations of the all, fine, and coarse mode aerosol single scattering albedo (SSA) at 550 nm (a) and the aerosol refractive indices at 440 nm (b) in urban area of Nanjing.

Figure 4. Frequency distributions of the ~~total (a), scattering (b), and absorbing aerosol (c)~~ size dependent AODs at 550 nm (a), AEs at 440/870 nm (b), SSAs at 550 nm (c) as well as the real and imaginary parts at 440 nm (c) ~~for the all (AOD, SAOD, AAOD), fine (FAOD, FSAOD, FAAOD) and coarse (CAOD, CSAOD, CAAOD) modes~~ in urban area of Nanjing.

~~Figure 5. Frequency distributions of the total (a), scattering (b), and absorbing aerosol (c) AEs at 440/870 nm for the all (AE, SAE, AAE), fine (FAE, FSAE, FAAE) and coarse (CAE, CSAE, CAAE) modes in urban area of Nanjing.~~

~~Figure 6. Frequency distributions of the all (SSA), fine (FSSA), and coarse (CSSA) mode aerosol SSAs at 550 nm (a) and the real and imaginary parts at 440 nm (b) in urban Nanjing.~~

Figure ~~7~~5. Comparisons between CE-318 and MODIS based AOD at 550 nm and between AE at 440/870 nm for CE-318 and at 412/470 nm for MODIS in Nanjing.

Figure ~~8~~6. Comparisons between the absorbing aerosol optical depth (AAOD) at 550 nm from CE-318

and surface absorption coefficient (AAC) at 520 nm from AE-31 (a) and between the column AAE at 440/870 nm from CE-318 and surface AAE at 470/880 nm from AE-31 (b) in urban Nanjing.

Figure ~~9~~7. The averaged aerosol volume size ($\mu m^3/\mu m^2$) distributions in different seasons (a) and in different AOD levels in urban Nanjing.

Figure ~~10~~8. Seasonal variations of the effective (a, μm) and mean (b, μm) radius of aerosols as well as the aerosol volume concentrations (c, $\mu m^3/cm^3$) in the all, fine and coarse modes in urban Nanjing.

Figure ~~11~~9. Relationships between the monthly mean values of 491 nm SSA and total Ångström exponent (AE) at 491/870 nm (a), between the monthly mean values of the real refractive index at 670 nm and AE at 491/870 nm (b), and between the monthly mean values of the SSA difference (870–491 nm) and AE at 491/870 nm (c).

Figure ~~12~~10. Distribution of the SSA and AAOD Curvatures in urban area of Nanjing under different spectral SSA conditions, including monotonically decreasing, increasing SSA spectra and peaked SSA spectra.

Figure ~~13~~11. The aerosol vertical proportions (%) from CALIPSO, Polarization-Raman Lidar and their average in Nanjing.

Figure ~~14~~12. Seasonal variations of the clear sky aerosol direct radiative forcing (DRF, W/m^2) at both TOA (a~c) and the surface (d~f). The DRFs of the total (a, d), scattering (b, e) and absorbing (c, f) aerosols in the all, fine and coarse modes are all investigated in urban Nanjing.

Figure ~~15~~13. Comparisons in the absorbing aerosol DRFs (W/m^2) between from BC SSA and from the total aerosol DRF minus the scattering one.

Figure ~~16~~14. Sensitivities of the TOA and the surface aerosol DRFs (day time, W/m^2) to the different aerosol profiles in clear conditions, for the total, scattering and absorbing aerosols.

Tables:

Table 1 Statistical summary of the columnar aerosol optical properties in urban area of Nanjing

Factors	Max	Min	Mean±SD	Meadian
550 nm AOD	2.3208	0.2723	0.6494±0.2852	0.5912
550 nm FAOD	2.2216	0.1468	0.5257±0.2806	0.4479
550 nm CAOD	0.9891	0.0139	0.1237±0.1076	0.0858
550 nm SAOD	2.2744	0.2443	0.6059±0.2747	0.5492
550 nm FSAOD	2.1459	0.1435	0.5014±0.2713	0.4263
550 nm CSAOD	0.8842	0.0113	0.1045±0.0957	0.0705
550 nm AAOD	0.2304	0.0020	0.0435±0.0240	0.0421
550 nm FAAOD	0.1424	0.0005	0.0244±0.0175	0.0208
550 nm CAAOD	0.1163	0.0009	0.0192±0.0145	0.0156
440/870 nm AE	1.9100	0.3085	1.2045±0.2856	1.2436
440/870 nm FAE	2.3625	0.3565	1.7083±0.2979	1.7364
440/870 nm CAE	-0.0789	-0.3805	-0.1876±0.0430	-0.1898
440/870 nm SAE	1.9916	0.2958	1.1976±0.3085	1.2386
440/870 nm FSAE	2.3653	0.3463	1.7102±0.2980	1.7368
440/870 nm CSAE	-0.1048	-0.7111	-0.3838±0.1017	-0.3864
440/870 nm AAE	3.4619	0.1483	1.3237±0.4820	1.2587
440/870 nm FAAE	4.5118	0.2912	1.7521±0.6470	1.6516
440/870 nm CAAE	3.1264	-0.0844	0.8748±0.4589	0.8209
550 nm SSA	0.9959	0.8053	0.9297±0.0335	0.9305
550 nm FSSA	0.9974	0.8388	0.9524±0.0261	0.9549
550 nm CSSA	0.9835	0.5898	0.8208±0.0754	0.8225
440 nm Real part	1.6000	1.3300	1.4423±0.0638	1.4374
440 nm Imaginary part	0.0301	0.0005	0.0084±0.0047	0.0078

AOD: Aerosol optical depth
FAOD: Fine aerosol optical depth
CAOD: Coarse aerosol optical depth
SAOD: Scattering aerosol optical depth
FSAOD: Scattering aerosol optical depth in fine mode
CSAOD: Scattering aerosol optical depth in coarse mode
AAOD: Absorbing aerosol optical depth
FAAOD: Absorbing aerosol optical depth in fine mode
CAAOD: Absorbing aerosol optical depth in coarse mode
AE: Ångström exponent of total aerosols
FAE: Ångström exponent of fine aerosols
CAE: Ångström exponent of coarse aerosols
SAE: Ångström exponent of scattering aerosols
FSAE: Ångström exponent of scattering aerosols in fine mode
CSAE: Ångström exponent of scattering aerosols in coarse mode
AAE: Ångström exponent of absorbing aerosols
FAAE: Ångström exponent of absorbing aerosols in fine mode
CAAE: Ångström exponent of absorbing aerosols in coarse mode
SSA: Single scattering albedo of total aerosols
FSSA: Single scattering albedo of fine aerosols
CSSA: Single scattering albedo of coarse aerosols

Table 2 Seasonal mean±SD of the columnar aerosol optical properties in urban area of Nanjing

Factors	MAM	JJA	SON	DJF
550 nm AOD	0.6788±0.2919	0.7508±0.3749	0.5866±0.2447	0.6560±0.2976
550 nm FAOD	0.4739±0.2613	0.6798±0.3793	0.5149±0.2462	0.5687±0.2978
550 nm CAOD	0.2048±0.1356	0.0710±0.0599	0.0717±0.0346	0.0873±0.0685
550 nm SAOD	0.6284±0.2835	0.7031±0.3728	0.5495±0.2342	0.6157±0.2829
550 nm FSAOD	0.4529±0.2552	0.6463±0.3760	0.4901±0.2366	0.5428±0.2846
550 nm CSAOD	0.1756±0.1225	0.0568±0.0497	0.0593±0.0315	0.0728±0.0601
550 nm AAOD	0.0503±0.0208	0.0477±0.0307	0.0372±0.0200	0.0403±0.0271
550 nm FAAOD	0.0211±0.0125	0.0335±0.0212	0.0248±0.0157	0.0259±0.0211
550 nm CAAOD	0.0292±0.0165	0.0142±0.0137	0.0124±0.0066	0.0144±0.0111
440/870 nm AE	0.9915±0.2385	1.2174±0.2639	1.3744±0.1907	1.3134±0.2461
440/870 nm FAE	1.7474±0.2896	1.4701±0.3075	1.7408±0.2582	1.6935±0.3019
440/870 nm CAE	-0.1998±0.0352	-0.1699±0.0471	-0.1862±0.0424	-0.1807±0.0464
440/870 nm SAE	0.9812±0.2687	1.2733±0.2950	1.3824±0.2043	1.2956±0.2697
440/870 nm SFAE	1.7555±0.2862	1.5218±0.3397	1.7492±0.2545	1.6809±0.3039
440/870 nm SCAE	-0.3752±0.0743	-0.2815±0.0678	-0.3797±0.0991	-0.4016±0.1162
440/870 nm AAE	1.1885±0.4500	0.7971±0.2657	1.3290±0.4533	1.5007±0.4520
440/870 nm FAAE	1.7352±0.6059	0.9943±0.2672	1.6715±0.5970	1.8947±0.6545
440/870 nm CAAE	0.8542±0.4665	0.3771±0.2753	0.8312±0.4479	0.9798±0.4235
550 nm SSA	0.9204±0.0313	0.9241±0.0422	0.9348±0.0331	0.9378±0.0331
550 nm FSSA	0.9527±0.0237	0.9405±0.0356	0.9518±0.0253	0.9555±0.0265
550 nm CSSA	0.8340±0.0628	0.7868±0.0953	0.8115±0.0752	0.8211±0.0810
440 nm Real part	1.4647±0.0628	1.4075±0.0609	1.4252±0.0602	1.4404±0.0582
440 nm Imaginary part	0.0084±0.0040	0.0083±0.0052	0.0080±0.0044	0.0083±0.0053

Table 3. The annual mean aerosol direct radiative forcing (W/m^2) in urban area of Nanjing

Species	Clear sky	
	TOA	Surface
TA	-10.69±3.37	-25.54±2.83
FA	-11.17±3.09	-21.37±2.78
CA	-0.33±0.60	-6.15±2.90
SA	-16.45±2.81	-17.17±2.96
FSA	-15.08±3.18	-15.74±3.35
CSA	-2.31±1.18	-2.42±1.24
AA	5. 76±1.27	-8.38±1.56
FAA	3.91±0.95	-5.63±1.16
CAA	1.99±1.07	-3.73±1.71

TA: Total aerosols

FA: Fine aerosols

CA: Coarse aerosols

SA: All scattering aerosols

FSA: Scattering aerosols in fine mode

CSA: Scattering aerosols in coarse mode

AA: All absorbing aerosols' forcing

FAA: Fine absorbing aerosols' forcing

CAA: Coarse absorbing aerosols' forcing

Figures:

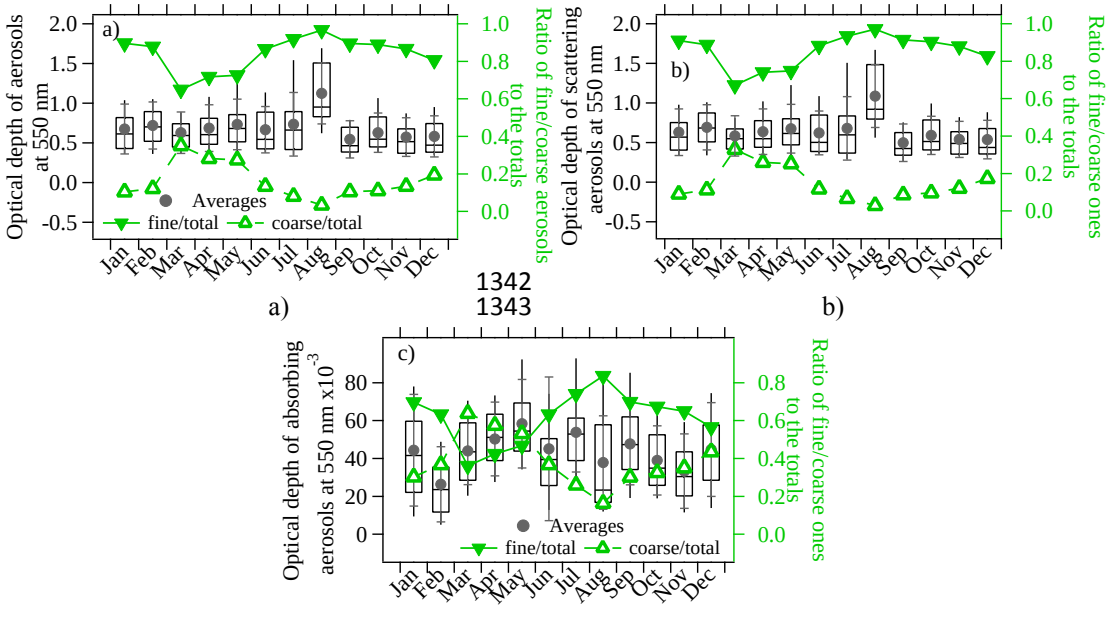

a) b) c)

Figure 1.

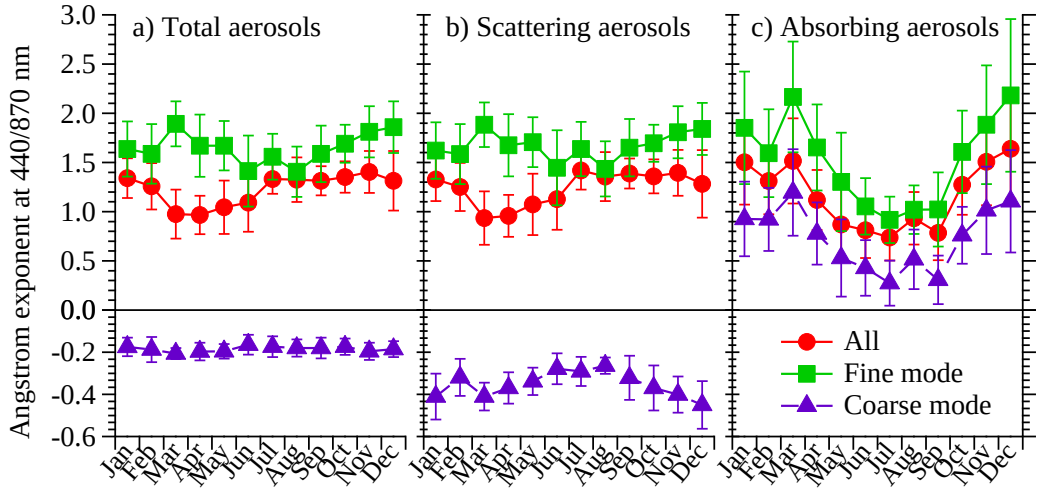

Figure 2.

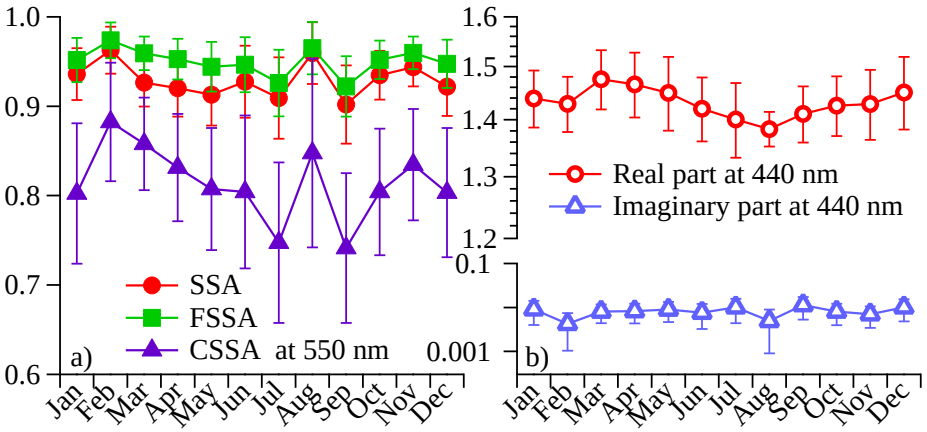

Figure 3

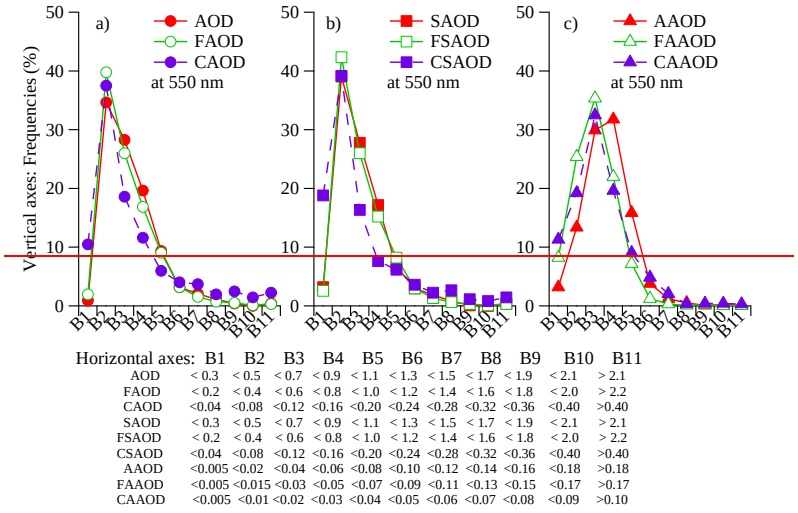

	B1	B2	B3	B4	B5	B6	B7	B8	B9	B10	B11
AOD	< 0.3	< 0.5	< 0.7	< 0.9	< 1.1	< 1.3	< 1.5	< 1.7	< 1.9	< 2.1	> 2.1
FAOD	< 0.2	< 0.4	< 0.6	< 0.8	< 1.0	< 1.2	< 1.4	< 1.6	< 1.8	< 2.0	> 2.2
CAOD	<0.04	<0.08	<0.12	<0.16	<0.20	<0.24	<0.28	<0.32	<0.36	<0.40	>0.40
SAOD	< 0.3	< 0.5	< 0.7	< 0.9	< 1.1	< 1.3	< 1.5	< 1.7	< 1.9	< 2.1	> 2.1
FSAOD	< 0.2	< 0.4	< 0.6	< 0.8	< 1.0	< 1.2	< 1.4	< 1.6	< 1.8	< 2.0	> 2.2
CSAOD	<0.04	<0.08	<0.12	<0.16	<0.20	<0.24	<0.28	<0.32	<0.36	<0.40	>0.40
AAOD	<0.005	<0.02	<0.04	<0.06	<0.08	<0.10	<0.12	<0.14	<0.16	<0.18	>0.18
FAAOD	<0.005	<0.015	<0.03	<0.05	<0.07	<0.09	<0.11	<0.13	<0.15	<0.17	>0.17
CAAOD	<0.005	<0.01	<0.02	<0.03	<0.04	<0.05	<0.06	<0.07	<0.08	<0.09	>0.10

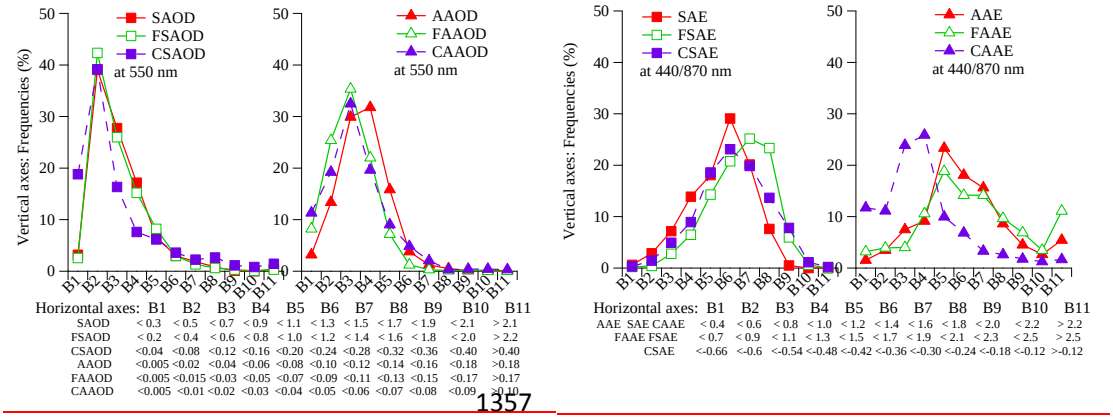

	B1	B2	B3	B4	B5	B6	B7	B8	B9	B10	B11
SAOD	< 0.3	< 0.5	< 0.7	< 0.9	< 1.1	< 1.3	< 1.5	< 1.7	< 1.9	< 2.1	> 2.1
FSAOD	< 0.2	< 0.4	< 0.6	< 0.8	< 1.0	< 1.2	< 1.4	< 1.6	< 1.8	< 2.0	> 2.2
CSAOD	<0.04	<0.08	<0.12	<0.16	<0.20	<0.24	<0.28	<0.32	<0.36	<0.40	>0.40
AAOD	<0.005	<0.02	<0.04	<0.06	<0.08	<0.10	<0.12	<0.14	<0.16	<0.18	>0.18
FAAOD	<0.005	<0.015	<0.03	<0.05	<0.07	<0.09	<0.11	<0.13	<0.15	<0.17	>0.17
CAAOD	<0.005	<0.01	<0.02	<0.03	<0.04	<0.05	<0.06	<0.07	<0.08	<0.09	>0.10

	B1	B2	B3	B4	B5	B6	B7	B8	B9	B10	B11
AAE SAE CAAE	< 0.4	< 0.6	< 0.8	< 1.0	< 1.2	< 1.4	< 1.6	< 1.8	< 2.0	< 2.2	> 2.2
FAAE FSAE	< 0.7	< 0.9	< 1.1	< 1.3	< 1.5	< 1.7	< 1.9	< 2.1	< 2.3	< 2.5	> 2.5
CSAE	<-0.66	<-0.6	<-0.54	<-0.48	<-0.42	<-0.36	<-0.30	<-0.24	<-0.18	<-0.12	>-0.12

a) b)

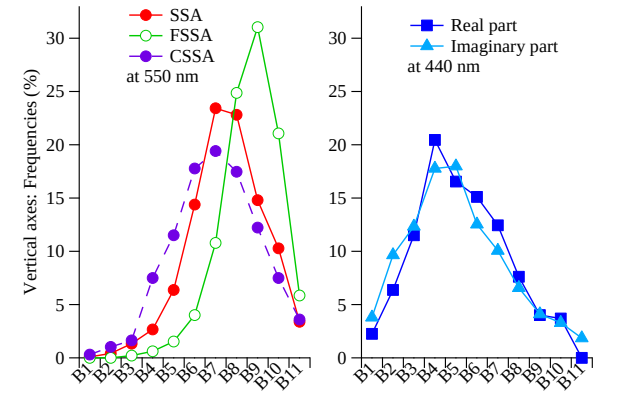

Horizontal axes:	B1	B2	B3	B4	B5	B6	B7	B8	B9	B10	B11
SSA FSSA	<0.81	<0.83	<0.85	<0.87	<0.89	<0.91	<0.93	<0.95	<0.97	<0.99	>0.99
CSSA	<0.60	<0.64	<0.68	<0.72	<0.76	<0.80	<0.84	<0.88	<0.92	<0.96	>0.96
Real	<1.33	<1.36	<1.39	<1.42	<1.46	<1.50	<1.54	<1.58	<1.62	<1.66	>1.66
Imag	<0.001	<0.003	<0.005	<0.007	<0.009	<0.011	<0.013	<0.015	<0.017	<0.019	>0.019

c)

Figure 4

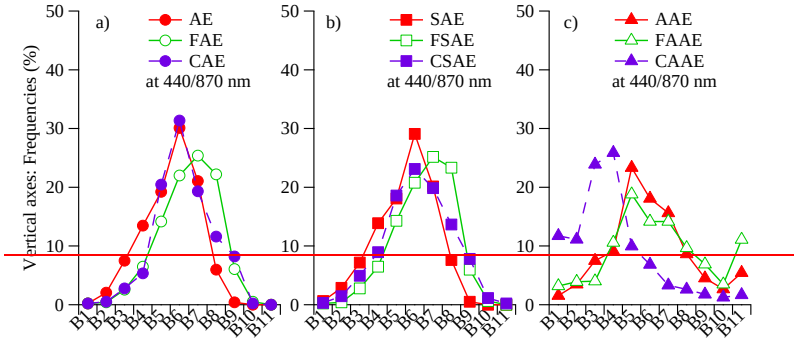

Horizontal axes:	B1	B2	B3	B4	B5	B6	B7	B8	B9	B10	B11
AE	< 0.4	< 0.6	< 0.8	< 1.0	< 1.2	< 1.4	< 1.6	< 1.8	< 2.0	< 2.2	> 2.2
FAE	< 0.7	< 0.9	< 1.1	< 1.3	< 1.5	< 1.7	< 1.9	< 2.1	< 2.3	< 2.5	> 2.5
CAE	<-0.33	<-0.3	<-0.27	<-0.24	<-0.21	<-0.18	<-0.15	<-0.12	<-0.09	<-0.06	>-0.06
SAE	< 0.4	< 0.6	< 0.8	< 1.0	< 1.2	< 1.4	< 1.6	< 1.8	< 2.0	< 2.2	> 2.2
FSAE	< 0.7	< 0.9	< 1.1	< 1.3	< 1.5	< 1.7	< 1.9	< 2.1	< 2.3	< 2.5	> 2.5
CSAE	<-0.66	<-0.6	<-0.54	<-0.48	<-0.42	<-0.36	<-0.30	<-0.24	<-0.18	<-0.12	>-0.12
AAE	< 0.4	< 0.6	< 0.8	< 1.0	< 1.2	< 1.4	< 1.6	< 1.8	< 2.0	< 2.2	> 2.2
FAAE	< 0.7	< 0.9	< 1.1	< 1.3	< 1.5	< 1.7	< 1.9	< 2.1	< 2.3	< 2.5	> 2.5
CAAE	< 0.4	< 0.6	< 0.8	< 1.0	< 1.2	< 1.4	< 1.6	< 1.8	< 2.0	< 2.2	> 2.2

~~Figure 5~~

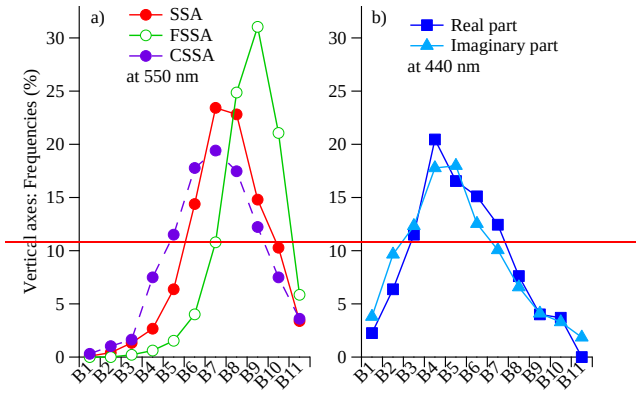

Horizontal axes:	B1	B2	B3	B4	B5	B6	B7	B8	B9	B10	B11
SSA	<0.81	<0.83	<0.85	<0.87	<0.89	<0.91	<0.93	<0.95	<0.97	<0.99	>0.99
FSSA	<0.81	<0.83	<0.85	<0.87	<0.89	<0.91	<0.93	<0.95	<0.97	<0.99	>0.99
CSSA	<0.60	<0.64	<0.68	<0.72	<0.76	<0.80	<0.84	<0.88	<0.92	<0.96	>0.96
Real	<1.33	<1.36	<1.39	<1.42	<1.46	<1.50	<1.54	<1.58	<1.62	<1.66	>1.66
Imag	<0.001	<0.003	<0.005	<0.007	<0.009	<0.011	<0.013	<0.015	<0.017	<0.019	>0.019

Figure 6

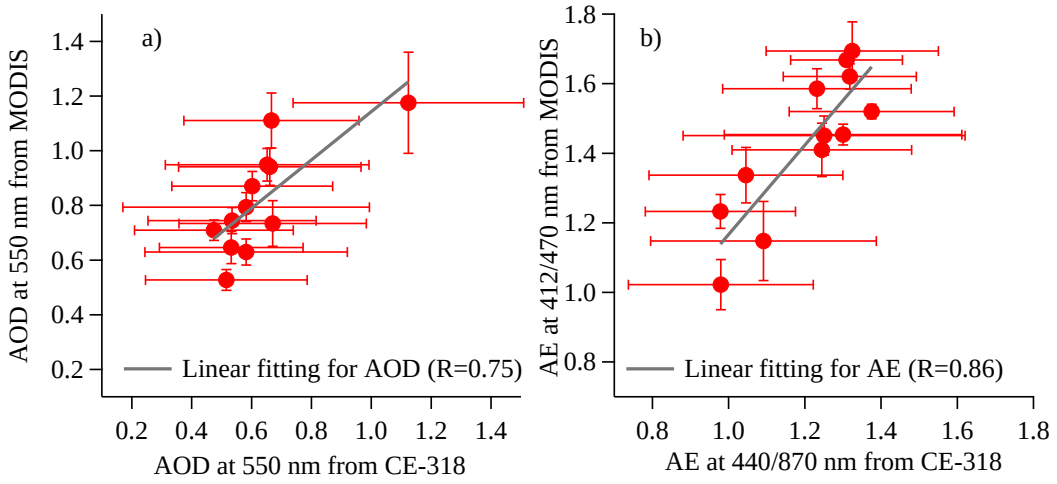

Figure 5

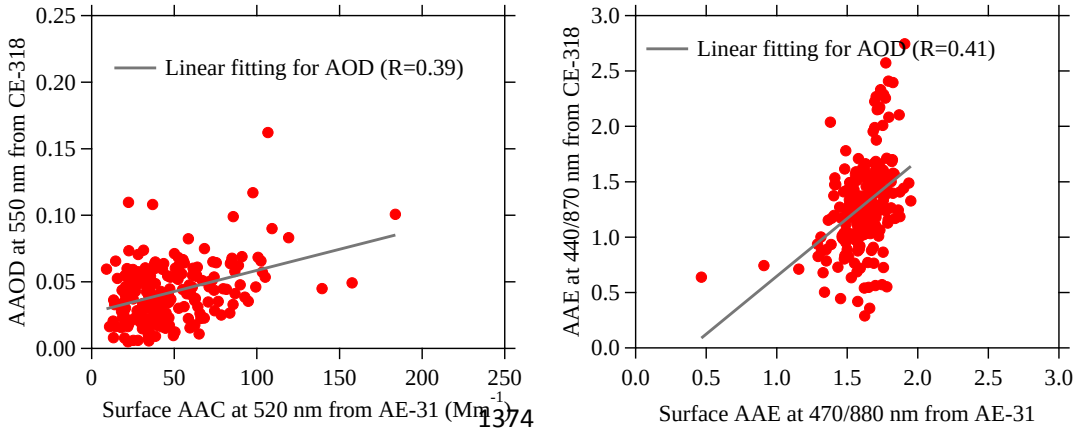

Figure 6

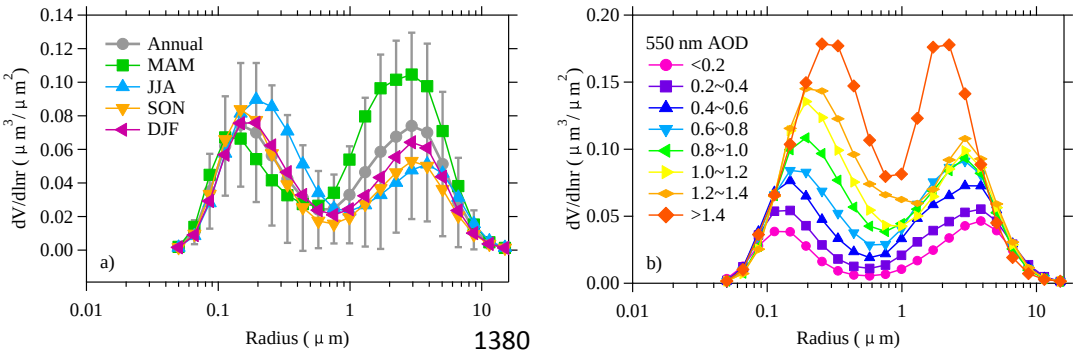

Figure 7

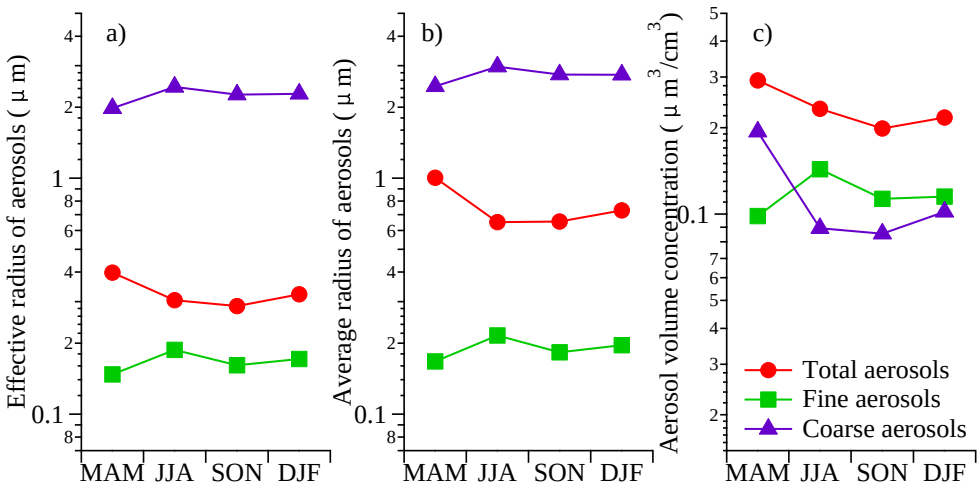

Figure ~~10~~8

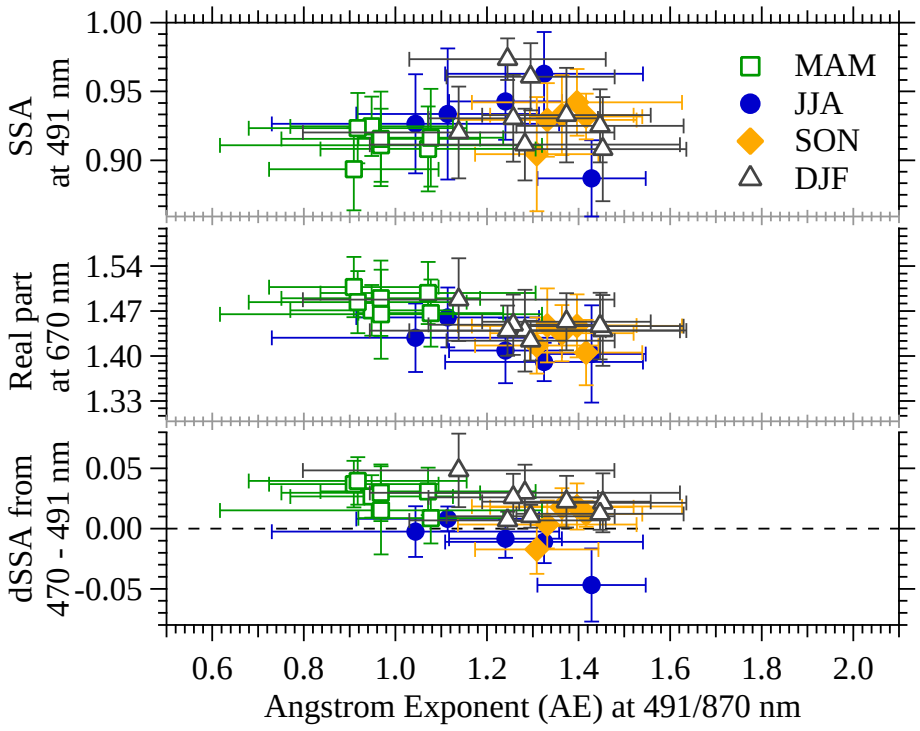

Figure ~~11~~9

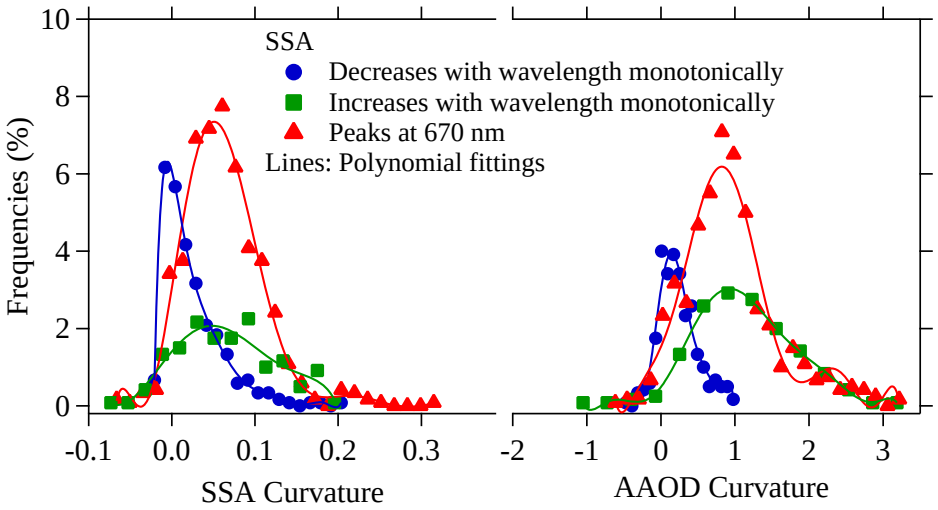

Figure ~~12~~10

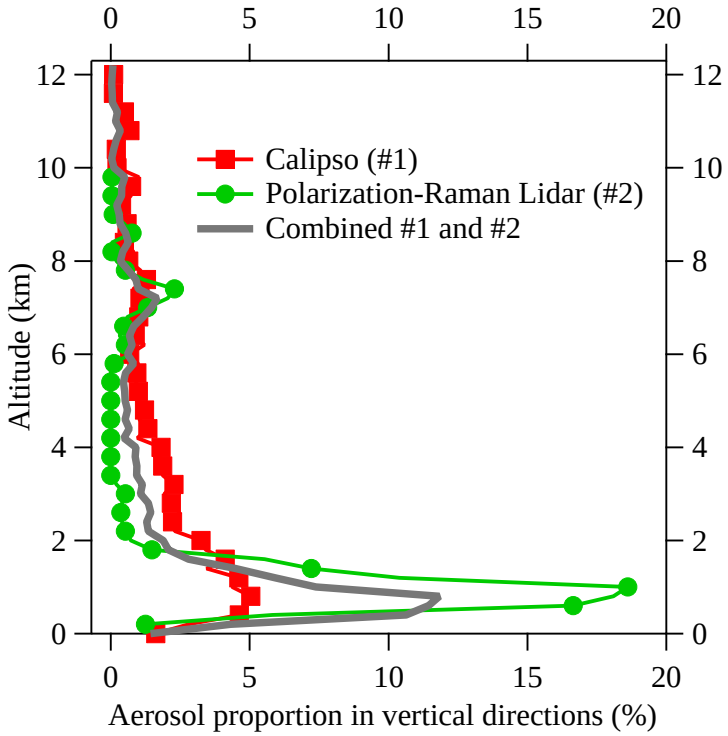

Figure ~~13~~11

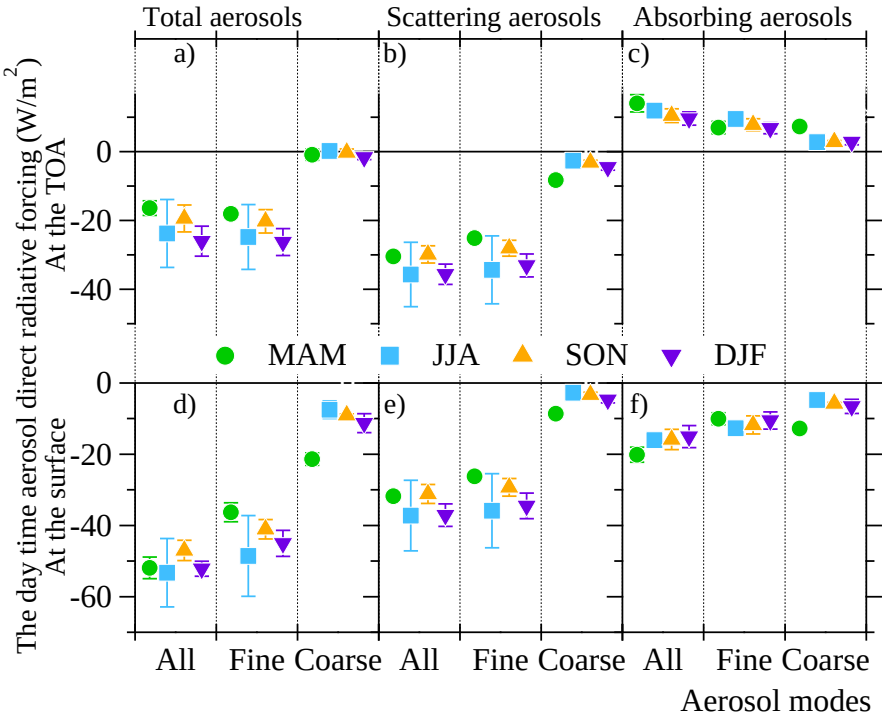

Figure ~~14~~12

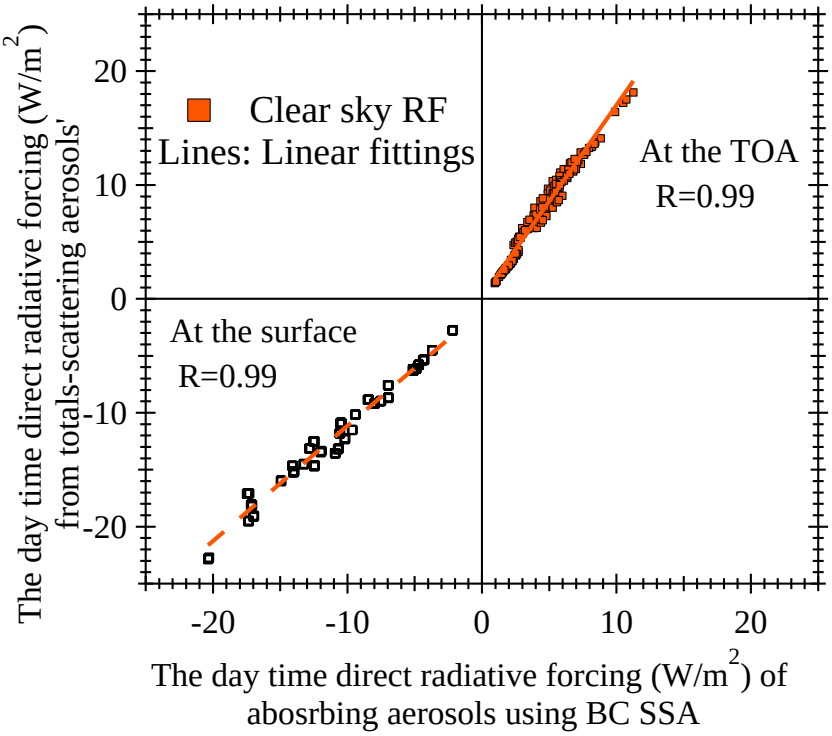

Figure ~~15~~13

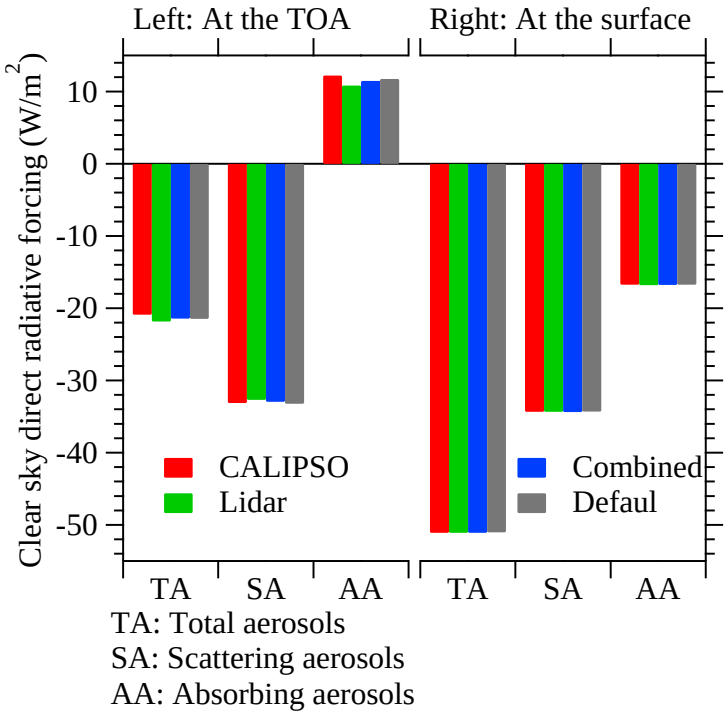
Left: At the TOA
Right: At the surface
Clear sky direct radiative forcing (W/m2)
10
0
-10
-20
-30
-40
-50
CALIPSO
Lidar
Combined
Defaul
TA
SA
AA
TA
SA
AA
TA: Total aerosols
SA: Scattering aerosols
AA: Absorbing aerosols

Figure ~~16~~14